

A Review of Traditional Multistage Roofs Design and Performance in Vernacular Buildings in Myanmar

Abstract

Myanmar's territory mostly experiences tropical monsoon climate, where temperatures are normally not extreme, but humidity can increase discomfort. In response, vernacular architecture strategies have evolved to deal with excess heat and humidity. One of the most prominent of these strategies is the use of high multistage roofs with ventilation. Over the years, many of the traditional buildings were altered but the use of multistage roof design has remained remarkably resilient in Myanmar. Nevertheless, little is known about their contribution to thermal comfort and their vulnerability to overheating risks due to the pervasive threat of the climate crisis.

In the work presented here, a thorough review of multistage roof typologies was followed by an investigation of their performance when building parameters including form, ventilation and materials were varied. Twenty-four dynamic simulations were performed using three building typologies and thirty-two fluid dynamic simulations were performed using two building typologies. In all cases, indoor volumes were kept the same. The results suggest that with the use of typical light-weight permeable envelope, the indoor temperatures follow ambient temperature closely; although a heavier-weight set of materials did not impact significantly on the maximum air temperatures, it has made a difference with regard to the lowest temperatures and overall comfort. The variable that impacted the most on the results was roof ventilation mode, with the best results being 3.5% of a year better than the worst. The multistage roof was found to help reduce heat gains from solar radiation.

The findings showed that Myanmar's vernacular buildings with multistage roofs offer an opportunity to improve indoor comfort in tropical climates and therefore its ability to moderate

indoor temperatures through the use of simple building physics and geometry should be honoured.

Keywords: Ancient Myanmar vernacular architecture; Building thermal performance; Natural ventilation; Roof typologies; IESVE and CFD; Building microclimates.

1. Introduction

The Asian country of Myanmar (also known as Burma) has an extensive territory that mostly experiences tropical monsoon climate with three seasons: cool (warm and dry, November to February), hot (very high temperatures but relatively dry, March to May) and rainy (hot and humid,). In response to this, and similarly to other countries with comparable conditions, vernacular architecture strategies have evolved to deal with excess heat and humidity. One of the most prominent strategies that can be commonly observed in Myanmar is the use of high multistage roofs with ventilation.

Over the years, Myanmar's vernacular architecture has undergone significant customisation such as changes in building forms, building plans, building materials and decorative features to meet a wide range of complex needs and social-economic limitations. Those changes in design have enabled the perpetuity of Myanmar vernacular architecture for many centuries; however, they have also raised a question of whether these buildings still deliver thermal comfort despite the alterations. Many of these traditional design features can be modified and implemented in modern buildings to improve their performance without the need for energy-hungry means of space conditioning and therefore are of extreme relevance when the need to mitigate and adapt to climate change is considered; nevertheless, this has not been studied to date.

Among many obstacles that have precluded it from being studied is the fact that it represents an alternative mode imposed by the enlightenment in Buddhism. Another obstacle is the rich diversity of the country and different customs between and within ethnic groups that have settled in Myanmar since 700 AD [1] as each of these groups have reflected their ethnicity on building characteristics. Early multistage roof design in Myanmar architecture can be traced to the archaeological pieces belonging to the Pagan (Bagan) period from the eighth century [2, 3]; thenceforth countless buildings have been designed using various forms of multistage roofs. In this paper, the authors present a detailed review of these and their evolution in Section 2. The use of multistage roof design seems to have remained remarkably resilient in Myanmar. However, little is known about their performance and therefore the authors have attempted to bridge this knowledge gap.

Myanmar was ranked second out of 183 countries in the long-term climate risk index for the period 1990-2018 [4, 5]. A past study revealed that a combination of traditional passive design techniques used in the Myanmar vernacular houses would not be sufficient to achieve thermal comfort in the present and predicted future climate scenarios [6, 7]. In the present work, the authors have focused particularly on the impact of multistage roofs in the performance of Myanmar's traditional buildings. Various building parameters including form and materials were investigated using dynamic whole-building simulation and computer fluid dynamics (CFD) in order to identify whether they are inherently vulnerable to overheating risks due to the pervasive threat of the climate crisis. Figure 1 presents the research method deployed in this study. The authors anticipate that this work will contribute to the ongoing resilience of Myanmar vernacular architecture.

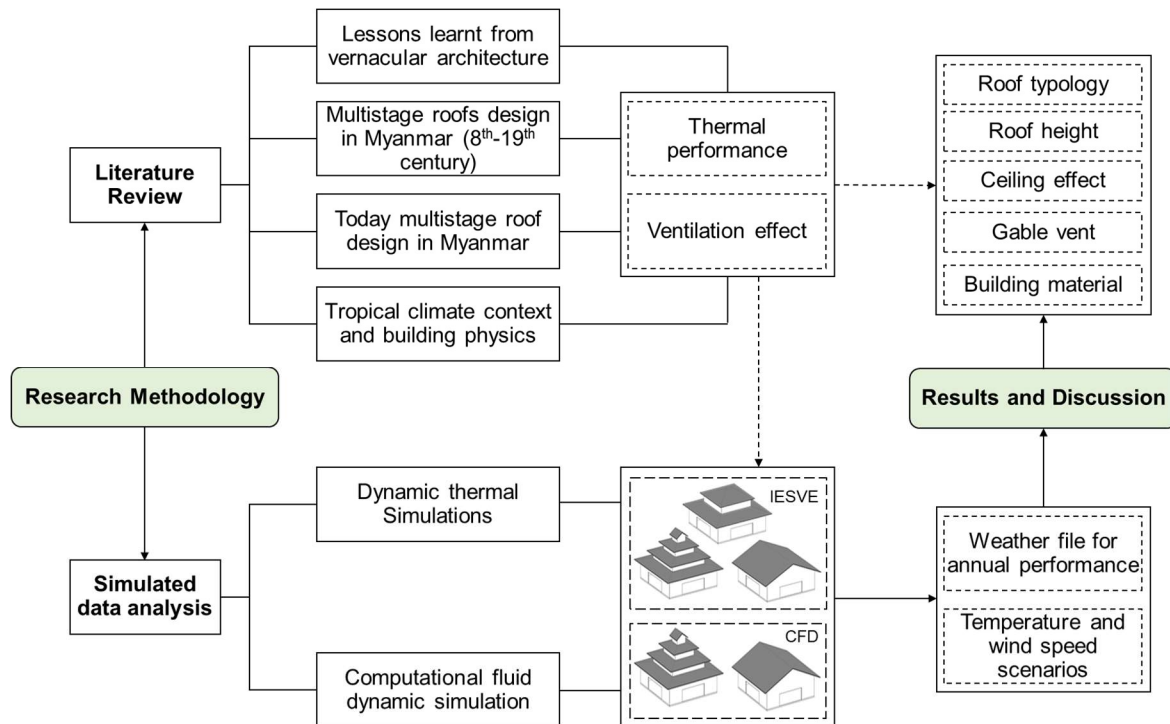


Figure 1. Research approaches and steps proposed and applied in this study

2. Context and Background

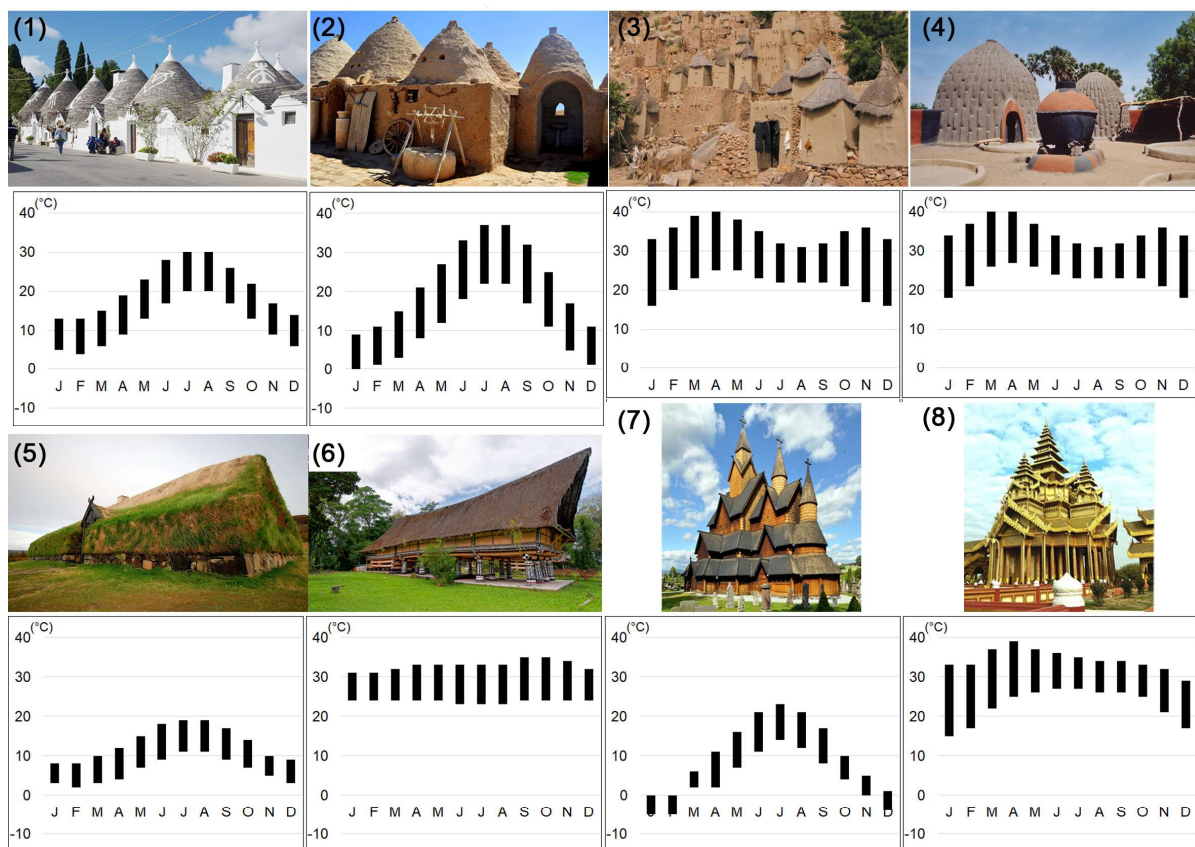
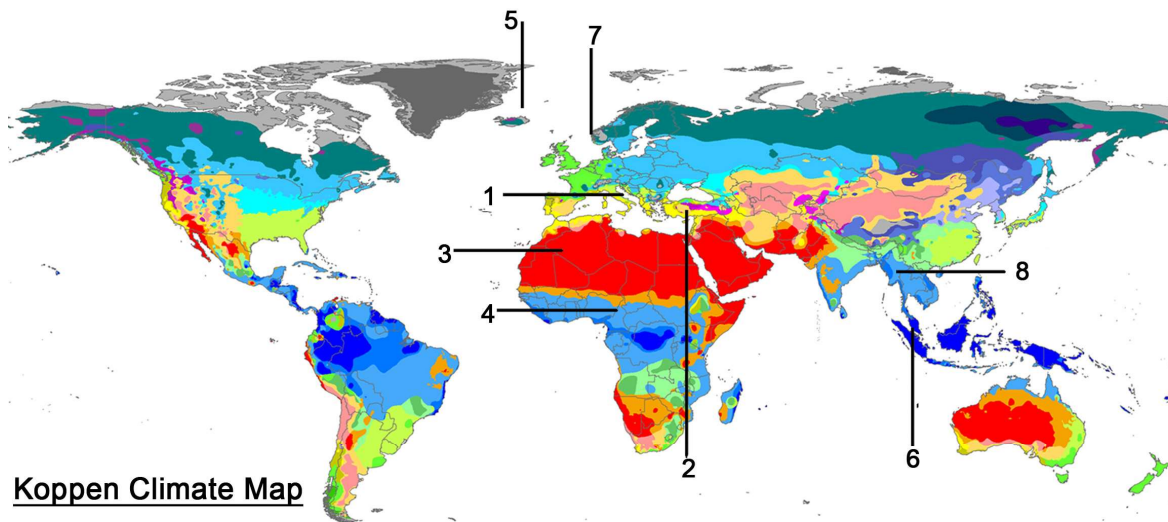
In this section, the authors first discuss what similarities and differences can be observed from vernacular architecture in general, from which the knowledge gained can be transferred to the Myanmar context. This is followed by a review of relevant historical and typological data that describes the transformation of the multistage roof design in Myanmar over time.

2.1. Lesson learnt from vernacular architecture

Despite variations in climates, culture and availability of construction materials, vernacular architecture from different locations share similarities [Figure 2]. For instance, the Trulli¹ house [8] and Beehive shape² houses [9, 10] are located at a 4° latitude difference and have a similar cone-shaped roof on a circular or square plan. However, different ventilation practices and uses of building materials create different microclimate modifiers for the two houses to maintain the indoor thermal comfort for their local contexts. Similarly, Mali houses in Dogon Country³ and Cameroon huts in Musgum⁴ [11] share similar beehive forms and homogeneous looks, but materials used and their interaction with the outdoor climates differ in order to maintain the indoor thermal comfort. Likewise, both Viking Stöng⁵ longhouses in

Iceland [12] and tropical Batak⁶ longhouses in Indonesia [13] share the same concept of longhouse shape layout and use of roof insulation, but ventilation practices differ in response to their outdoor climatic conditions. Despite 20°C temperature differences in their annual temperature profiles, Stave churches⁷ in north-western Europe and traditional buildings with multistage roofs in Myanmar still show similarities in the use of a series of roofs with wood structures.

Typically, additional heating is required for Nordic climates, and additional cooling is required for tropical climates. Therefore, despite similarities of roof design and materials used, many of the passive design techniques found in both types of vernacular architecture in order to maintain favourable building microclimates for indoor thermal comfort are different. In the Nordic conditions, it is necessary to control heat loss and this is usually done by using an airtight envelope with a smaller overall window area [14]. In contrast, in the tropics, it is necessary to control solar heat gain so large eave roof shading, and highly permeable building envelopes are observed, in addition to numerous openings, which are essential to achieve appropriate levels of natural ventilation for passive cooling [15, 16]. Design of stave churches and Myanmar's traditional buildings with multistage roofs have a parallel development in their historical timelines even though there appear to be no links between them. In sum, the vernacular architecture reviewed above – although by no means an exhaustive list - show how builders in the past used forms and materials effectively to moderate indoor conditions in their buildings and protect against extreme and prevailing climatic conditions.



1. Trulli of Alberobello, Bari, Italy
2. Beehive Houses of Harran, Turkey
3. Cliff of Bandiagara, Mali
4. Mugsum Mud Huts, Cameroon
5. Stöng Viking Longhouse, Iceland
6. Batak house, Indonesia
7. Stave church, Norway
8. Pyatthat, Myanmar

Figure 2. Some vernacular houses in Asia, Africa and Europe [17] and their location's monthly temperature variations [18, 19]

2.2. Buildings with multistage roofs in Myanmar

Myanmar is sandwiched between two of the most important civilizations in Asia – India in the north-west and China in the north-east. On the western side is a long coastline, while the

country itself extends through 18 degrees of latitude; as a result, Myanmar's climate ranges from the subtropical highland climate at the snow-covered mountain peaks in the north to tropical monsoon climate in the south. In between these extremes is a dry zone, corresponding to the equatorial winter dry climate to the mixed humid subtropical climate [20].

The multistage roofs are known as "*Pyatthat*"⁸ in Myanmar. Their use was initially restricted by the sumptuary laws to religious buildings for the continuity of the Buddhist tradition and the royal family; that context typifies a close link between Buddhism and kingship in forming the cultural heritage of Myanmar [3, 16, 21, 22]. Multistage roofs, which are dominant features of Myanmar's ancient traditional buildings, are made of successive gabled rectangular roofs in an exaggerated pyramidal shape that consists of a series of tiers [16]. The form is a fixed kind of 'parasol' concept; therefore, a roof can be thought of as a broad umbrella over the occupied spaces. The use of an abstract roof curve defines the shape of multistage roofs to divide the number of tiers. The number of tiers in the buildings with multistage roofs represents Buddhist cosmology – the description of the 31 planes of existence. The centre of multistage roofs is recognised as the hallmark of a building – a place for either the image of the Buddha or the throne room of a king [2, 16]. An intermediate box-like roof structure inserted between each tier is called *Le-baw*, where gable vents are added for roof ventilation. The total building height, including the height of the raised floor and the crown of the multistage roofs, varies between 1.25 and 2 times the length or width of the building. Four types of multistage roof, shown in Figure 3, are categorised by historical dynasties⁹ [2].

From the fifteenth century Bargayar monastery [Figure 3] to the eighteenth century Mandalay palace and Myadaung monasteries [Figure 4], most of the surviving buildings with multistage roofs can be found around Mandalay [3, 16]. Towards the end of the eighteenth century or in the early nineteenth century, several changes in the buildings with multistage roofs could be observed due to the impacts of socio-economic and political conditions. For

instance, a colourful Italianate façade, further uplifted by tiered teak roofs, is one of the finest examples of brick and plaster monasteries [Figure 4] showcasing changes in building technology with the novel forms of cultural expression in the 1930s [3].

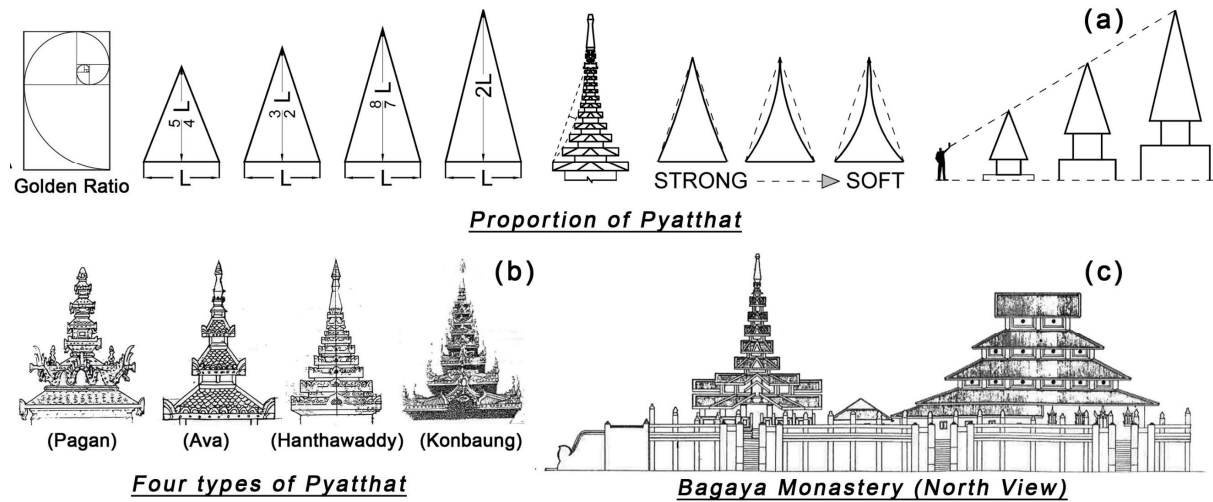


Figure 3. (a) Proportion of Pyatthat (b) Four types of Pyatthat [2] (c) Bagaya monastery in Mandalay (completed in 1593) [16]

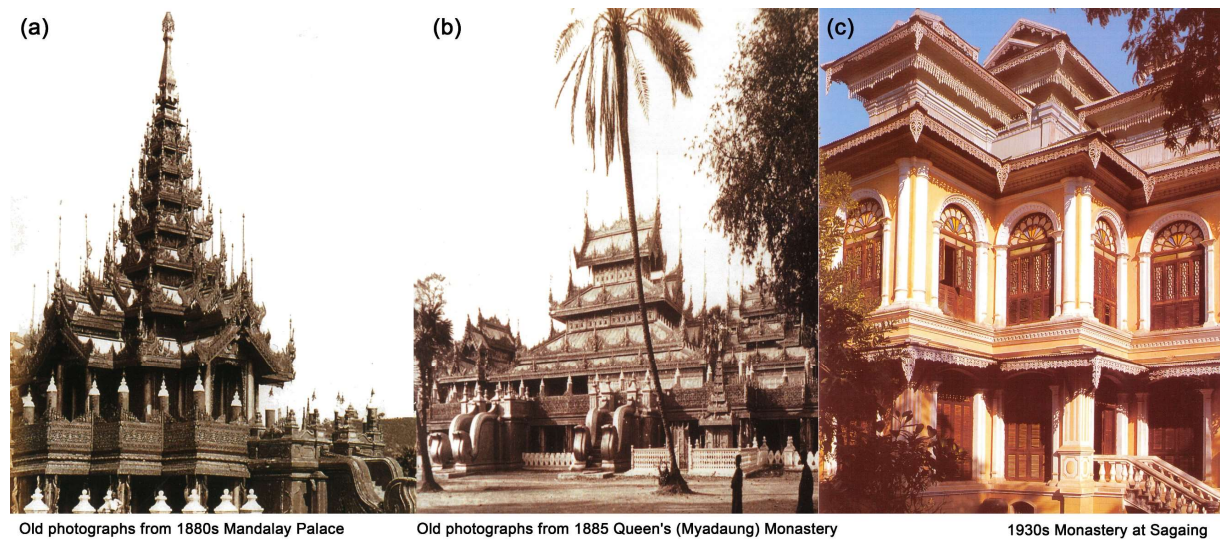


Figure 4. (a) Mandalay Palace in the 1880s; (b) Myadaung monasteries in 1885; (c) Monastery at Sagaing in the 1930s [3]

Today, the traditional tiered roof features of Yangon city hall [23], the concourses of Bagan Airport and the Naypyidaw Parliament building [24] represent the use of multistage roofs as memorable treasures of Myanmar traditional architecture. The Karaweik Hall palace [3] and the elaborate wooden resting pavilion in the Novotel Mandalay hotel [3] represent multistage roof-inspired building forms as an echo of Myanmar architecture. Kandawgyi Palace Hotel completed in 1996 by a Thai Architects firm [3] reveals the sharing concept of a

series of roofs between Myanmar and Thailand as contemporary architecture. It also can be seen that the relics of building form remain up to the present day as both traditional and contemporary architecture, and their presence represents material fragments of historical reality.



Figure 5. The use of multistage roof in Myanmar architecture [3, 23, 24]

2.3. Tropical climate context in multistage roof design

Tropical climate zones are found in the regions between the equator and the tropics, where the general patterns of the climates are typically frost-free and warm, and where humidity is variable depending on the precipitation pattern. Sunlight is intense in the tropics and the intensity of diffuse solar radiation is high. Tropical vernacular architecture employs natural ventilation and sun protection in order to respond to these climatic characteristics for building thermal performance. Deep overhangs, pitched thatch roofs with high insulation and verandas allow a building to buffer the direct solar heat gain. Raised high floors help to increase airflow around and under a building, and highly permeable building envelopes with lightweight timber and bamboo walls offer improved ventilation. A number of windows including gable vents are typical tropical vernacular design features. These can be seen in many Asian houses including Myanmar vernacular houses [6, 25].

Figure 3, 4 and 5 show that there have been several changes in forms and use of materials in Myanmar's traditional buildings with multistage roofs over time. Original thatch and timber shingles have become metal roofs, and timber walls and raised timber floors have become brick walls and concrete floors. Open corridors along with the perimeter of the building were often lost due to the constraints of the gross floor area. The numbers of the occupied storey have increased, and the height of raised floors was lost. Despite the changes, the multistage roofs in Myanmar's traditional buildings have stayed remarkably resilient.

In Figure 6, a comparison between three roof typologies with the same internal volume but varied roof height is shown. Building (a) has a combination of hipped-roofs and multi-tier roofs [Figure 6-a] distributed on four sides, and the shape of the roof dictated the height and indoor air volume. In order to keep the same internal air volume as in building (a), in building (b) a combination of multi-tier and offset gable roofs was used to reduce the roof height and increase the width [Figure 6-b]. In building (c) [Figure 6-c], the length of the intermediate roof structures was kept the same so it was necessary to reduce the height of the roof in order to maintain the same internal air volume. The use of intermediate roof structures in the building (b) and (c) is not as significant as their use in building (a). This simple comparison also indicated that the investigation of various practices in roof typologies is, indeed, a wide scope of work. However, one obvious investigation can be done by comparing building (a) – an original multistage roof design from the Pagan dynasty – and a building with a single gable roof, from which the impacts of roof height and the use of intermediate roof structures on the thermal performance can be investigated.

Vernacular architecture strategies are microclimate modifiers [26]. By building microclimate we mean the combination of the indoor microclimate and the surrounding microclimate, and therefore this is considered an extension of the indoor climate [27]. Spaces which are connected either horizontally or vertically are, therefore, building microclimate

modifiers. Elevated naves in the stave churches and roof spaces in Myanmar's traditional buildings with multistage roofs can be counted as one type of building microclimate modifier. Therefore, it is important to investigate how the changes in roof typologies, roof height, roof ventilation and building materials affect building microclimate for thermal performance of a building with a multistage roof.

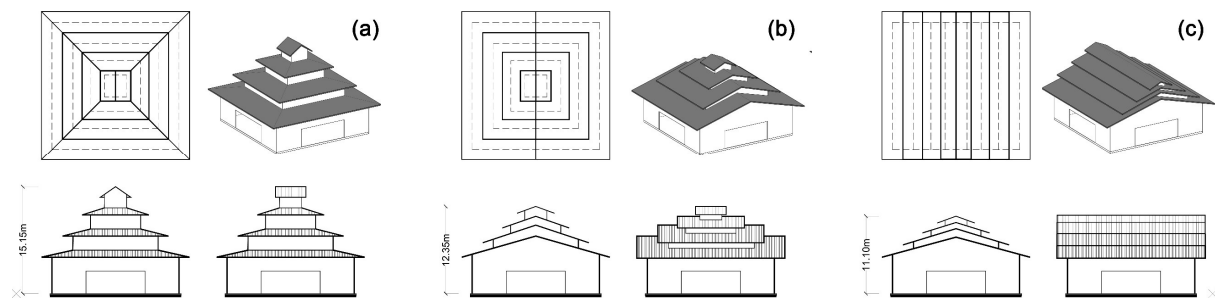


Figure 6. Building with multistage roofs (a) hipped roofs and multitier; (b) offset gable roofs and multitier; (c) same length gable roofs and multitier

3. The simulation studies

In order to evaluate the contribution of each roof typology, roof height, roof ventilation and building materials on the thermal performance of a building with a multistage roof, the authors set the following key questions:

1. How does varying the building envelope materials affect the thermal performance of the different roof typologies?
2. Which roof typology is more effective in reducing the indoor air temperature?
Which roof typology has the most effective indoor airflow?
3. To what extent can the building with multistage roofs improve the indoor thermal environment?

In order to isolate the key variables, the buildings were modelled with a single zone using dynamic thermal simulation and computational fluid dynamics simulation (CFD) programmes. The dynamic thermal simulations focused on investigating the resultant overall indoor air temperatures of three building typologies [Figure 7] with various conditions. The CFD

simulations focused on investigating the air temperatures and airflows of two building typologies [Figure 8].

3.1. Dynamic thermal simulation

Simulation engine: The simulations were performed using the Integrated Environmental Solution software (IES, version 2019 Hotfix1), a commercially well-known software, which specialises in building performance analysis and qualifies as a dynamic model in the Chartered Institution of Building Services Engineers (CIBSE) classification system. ApacheSim, a dynamic thermal simulation program in IES, uses first-principles mathematical modelling of the heat transfer processes occurring within and around a building. MacroFlo, which runs as an adjunct to ApacheSim by exchanging data at run-time, generates a fully integrated simulation of air and thermal exchanges for one weather year [28].

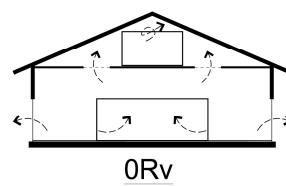
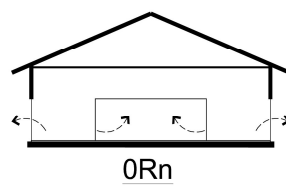
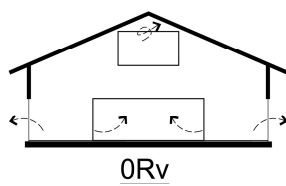
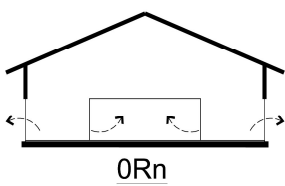
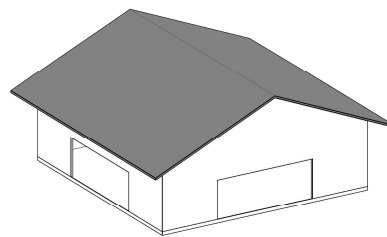
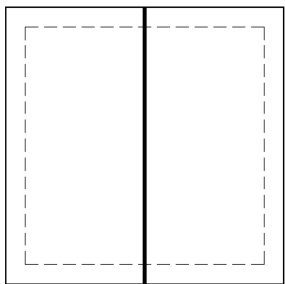
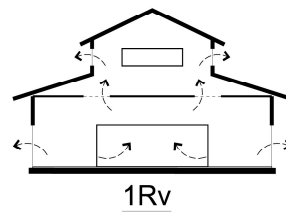
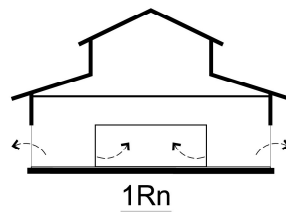
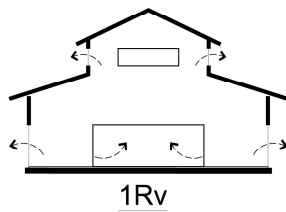
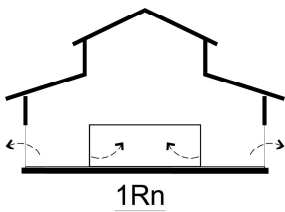
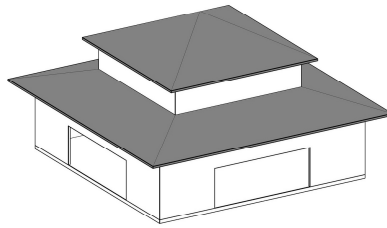
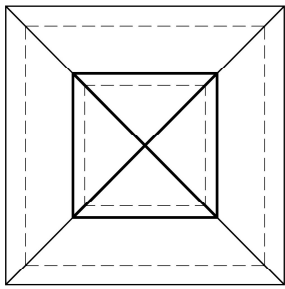
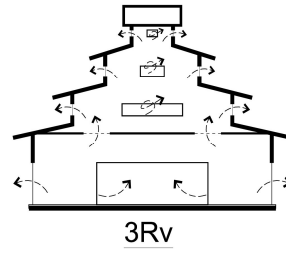
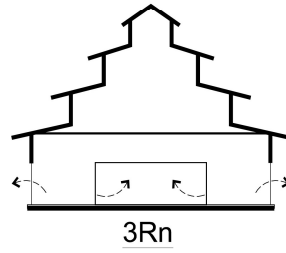
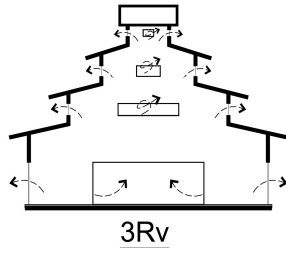
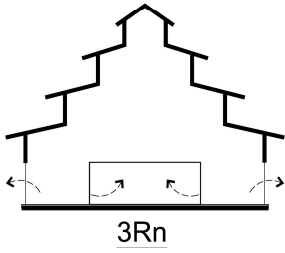
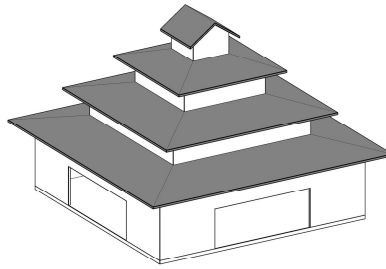
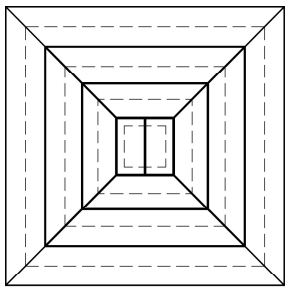
Building geometry: A building with a three-stage hipped roof (3R), a building with a one-stage hipped roof (1R) and a building with a single gable roof (0R) were used in the dynamic thermal simulation. Regarding the geometries of the buildings [Figure 7], the sizes of the occupied space were first fixed as 18m length, 18m width, and 5m height. The combined heights of the building were then set as 15.15m in building 3R; the total height of buildings 1R and 0R were, therefore, lower than building 3R. The size of the intermediate roof structures was increased in building 1R to retain the same internal air volume. The characteristics of the building geometries and building abbreviations, as shown in Figure 7 and Table 1, mean that the internal air volumes of each building were fixed, but the heights of the three buildings were different. Regarding the abbreviations that describe the models, the suffix 'n' represents the buildings with no gable vents in the roof structures and the suffix 'v' represents the buildings with gable vents in the roof structures.

Opening: In the occupied spaces of all buildings, a total of 108 m² (equivalent to 30% of the window-to-wall-area-ratio of the occupied space) for the fenestration areas was equally

distributed across all four sides of the walls. Additionally, the gable vent area 23.92 m^2 was equally split into all the roof stages of the buildings 3Rv, 1Rv and 0Rv. Geometrically, there were 12 scenarios shown in Figure 7 – three roof typologies, two ventilation modes, and two ceiling modes. The ceiling modes were the buildings with ‘no ceiling’ and the buildings ‘with ceilings’ added. For the latter mode, a $600 \times 600 \text{ mm}$ size ceiling void at every 6m intervals was added in each building to remove the air through the gable vents. Regarding the opening time for fenestration, the fenestration of occupied space from all buildings was opened from 06:00 a.m. to 18:00 p.m., which means they were opened during the daytime. The gable vents in the roof spaces were continuously open.

Internal gains: In order to simplify the effects of internal gains in the CFD simulations, the dynamic thermal simulations for all buildings were generated with no internal gains from the occupants, equipment or lighting. Myanmar’s vernacular buildings are a free-running building type; therefore, both simulations were generated by using natural ventilation mode.

Materials and simulation scenarios: The 12 scenarios doubled when two sets of building materials were considered for the building envelopes as shown in Table 3 (see Appendix). Therefore, there were a total of 24 scenarios due to variations in typologies, ceiling modes, building materials, and ventilation modes. The material set-1 contained thatch roofs, timber floors, timber walls, timber ceilings, and timber windows. The material set-2 contained metal roofs, concrete floors, brick walls, timber ceiling, and glazed windows. One needs to note that the buildings shown in Figure 7 and Table 1 are those with material set-2. Therefore, the total building height for each building of the material set-1 will be 3m higher than the material set-2 because of the raised floor height for a timber floor. The infiltration was set as 10 ac/h for the buildings with material set-1 and 1.5 ac/h for the buildings with material set-2, which were rough assumptions [6, 29]. The results of dynamic thermal simulations were compared with the results of computational fluid dynamics simulations.



Buildings with 'no ceilings' mode

Buildings with 'ceiling added' mode

Figure 7. Twelve building typologies used in the dynamic thermal simulations, material set-2.

Table 1. Geometry characteristics of the buildings used in both simulations

Buildings	Gable Vents contained	Building Height	Window Areas (m ²)	Gable Vents Areas (m ²)	Room air volume (m ³)
3Rv	Yes	15.150	108	23.92	2450
3Rn	No	15.150	108	0.00	2450
1Rv	Yes	11.925	108	23.92	2450
1Rn	No	11.925	108	0.00	2450
0Rv	Yes	9.525	108	23.92	2450
0Rn	No	9.525	108	0.00	2450

Weather file: Most of the surviving buildings with multistage roofs can be found in Mandalay (21°58'N 96°5'E), the last royal capital of Myanmar, located in the central dry zone of the country. Therefore, the authors decided to use the Mandalay typical weather file for dynamic thermal simulations. Long-term historical weather data and future weather data are generally unavailable or very limited in Myanmar. The typical weather file used in this paper was generated by [Huang et al. \(2014\)](#) for the standard data of the American Society of Heating, Refrigerating and Air-Conditioning Engineers (ASHRAE) for simulation. The typical weather dataset was created with data collected from 2005 to 2013, less than a decade's worth. The study also [\[6\]](#) used the same weather files.

3.2. Computational fluid dynamics simulations

Numerical modelling method: The numerical simulations were carried out using ANSYS FLUENT 18.1 software. The assumptions for the steady-state simulation comprised a three-dimensional, fully turbulent and incompressible flow. The turbulent nature of the flow was modelled by the standard K-epsilon turbulence model ($k-\epsilon$) which is well established in the field of natural ventilation and windcatcher research [\[31, 32\]](#). The CFD code used the Finite Volume Method (FVM) approach and employed the Semi-Implicit Method for Pressure-Linked Equations (SIMPLE) velocity-pressure coupling algorithm with the second-order upwind discretisation. The simulations were completed using parallel processing on a workstation with two Intel Xeon 2.8GHz processors and a 64GB fully buffered DDR2.

CFD theory: The governing equations for the 1-continuity, 2-momentum, 3-energy, 4-turbulent kinetic energy (TKE) and 5-energy dissipation rate are detailed below:

$$\frac{\partial \rho}{\partial t} + \nabla \times (\rho U) = 0 \quad [1]$$

where ρ is density, t is time and U is the fluid velocity vector.

$$\frac{\partial(\rho u)}{\partial t} + \nabla \times (\rho u u) = -\nabla p + \nabla \times (\mu \nabla u) - \nabla \times \tau_t \quad [2]$$

where p is the pressure, g is a vector of gravitational acceleration, μ is molecular dynamic viscosity and τ_t is the divergence of the turbulence stresses which accounts for auxiliary stresses due to velocity fluctuations.

$$\frac{\partial(\rho e)}{\partial t} + \nabla \times (\rho e u) = \nabla \times (k_{eff} \nabla T) - \nabla \times (\sum_i h_i j_i) \quad [3]$$

where e is the specific internal energy, k_{eff} is the effective heat conductivity, T is the air temperature, h_i is the specific enthalpy of fluid and j_i is the mass flux.

$$\frac{\partial(\rho k)}{\partial t} + \nabla \times (\rho k u) = \nabla \times [\alpha_k \mu_{eff} \nabla k] + G_k + G_b - \rho \varepsilon \quad [4]$$

$$\frac{\partial(\rho \varepsilon)}{\partial t} + \nabla \times (\rho \varepsilon u) = \nabla \times [\alpha_\varepsilon \mu_{eff} \nabla \varepsilon] + C_{1\varepsilon} \frac{\varepsilon}{k} (G_k + C_{3\varepsilon} G_b) - C_{2\varepsilon} \rho \frac{\varepsilon^2}{k} \quad [5]$$

where G_k is the source of TKE due to average velocity gradient, G_b is the source of TKE due to buoyancy force, α_k and α_ε are turbulent Prandtls numbers, and $C_{1\varepsilon}$, $C_{2\varepsilon}$ and $C_{3\varepsilon}$ are empirical model constants. The Discrete Ordinates (DO) radiation model solves the radiative transfer equation [6] for a finite number of discrete solid angles, each associated with a vector direction \vec{s} fixed in the global Cartesian system (x, y, z):

$$\nabla \cdot (I(\vec{r}, \vec{s}) \vec{s}) + (a + \sigma_s) I(\vec{r}, \vec{s}) = a n^2 \frac{\sigma T^4}{\pi} + \frac{\sigma_s}{4\pi} \int_0^{4\pi} I(\vec{r}, \vec{s}') \varphi(\vec{s} \cdot \vec{s}') d\Omega' \quad [6]$$

where \vec{r} is the position vector; \vec{s} is the direction vector; \vec{s}' is the scattering direction vector; a is the absorption coefficient; n is the refractive index; σ is the scattering coefficient; σ_s is the Stefan-Boltzmann constant ($5.672 \times 10^{-8} \text{ W/m}^2\text{-K}^4$); I is the radiation intensity; φ is the phase function, and Ω' is the solid angle.

Boundary conditions: The boundary conditions for the flow study are specified in accordance with the best practice guidelines. The profiles for the airflow velocity U and

turbulent kinetic energy (TKE) are imposed at the inlet, with the stream-wise velocity of the incident airflow following the power law with an exponent equal to 0.14 corresponding to flow on a sub-urban terrain [Figure 16 of the Appendix]. The values of ϵ of the k- ϵ turbulence model are determined by assuming local equilibrium of $Pk = \epsilon$. Standard wall functions are invoked to all wall boundaries aside from the ground boundary, with the ground having wall functions adjusted for roughness. According to Cebeci and Bradshaw [33], this must be indicated by a corresponding sand-grain roughness height k_s and a roughness constant C_s . The horizontal non-homogeneous of the ABL is controlled by adapting sand grain roughness height and roughness constant for the inlet profile, adhering to the equation:

$$k_s = \frac{9.793z_0}{C_s} \quad [7]$$

where, z_0 is the aerodynamic roughness length corresponding to sub-urban terrain. The values selected for sand-grain roughness height and a roughness constant are 1.0 mm and 1.0, respectively, in accordance with best practice guidelines. The sides and the top of the domain are specified as symmetry, signifying zero normal velocity and zero gradients for all the variables in these boundary zones. Zero static pressure is used for the outlet boundary. The boundary conditions are summarised in Table 4 (see Appendix).

CFD Domain: If the building height was H , the inlet of the computational domain was $3H$ away from the building, and the outlet was positioned $15H$ behind the building, which is derived from Franke et al. [34]. The inlet wind speed profile was defined according to the logarithmic law of the wall for high Reynolds numbers for turbulent flow. All CFD models were sited on the ground surface with roughness height (K_s) = 0.14m and the constant roughness (C_s) = 7, which are derived from to Blocken et al. [35]. The simulation models were generated using medium grids and the unstructured mesh that allowed for flexibility in conforming to the complex geometries. The average skewness and the mesh quality for all models are shown in Table 5 (see Appendix). The turbulent nature of the flow was modelled

by the standard $k-\epsilon$ turbulence model and Reynolds Averaged Navier Stokes equations (RANS), which are well established in the field of fluid dynamic and heat transfer parameters [36, 37].

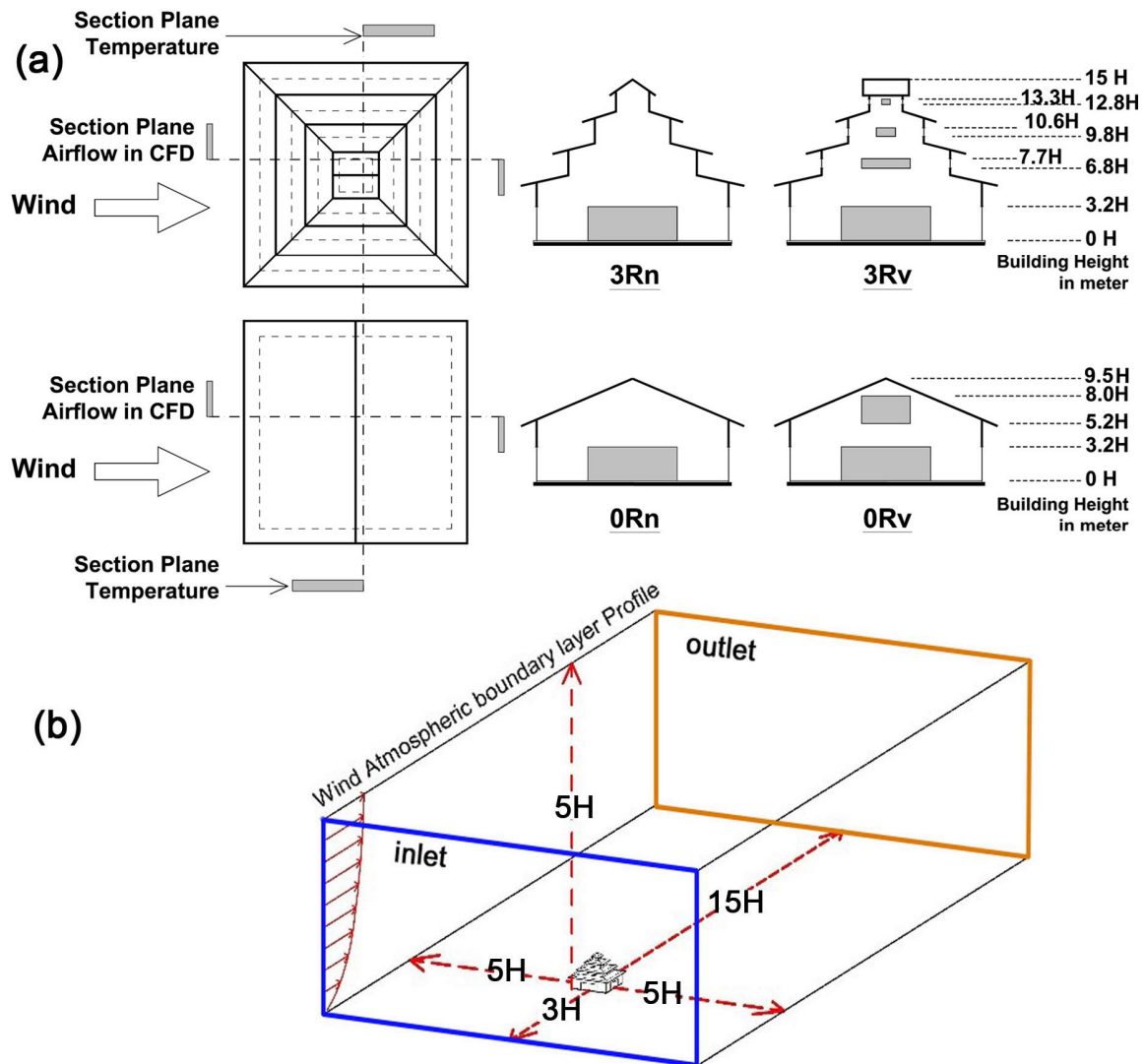


Figure 8. (a) Two building typologies used in the CFD simulations (b) Perspective view of the computational domain

Solution convergence: The solution convergence was monitored, and the solution was considered complete upon observation of no significant change between iterations. In addition, property conservation is also verified if attained. This is conducted by performing a mass flux balance for the converged solution. This option is available in the FLUENT flux report panel, which permits the computation of mass flow rate for boundary zones. For this study's

simulation, the mass flow rate balance is below the required value or $< 1\%$ of the smallest flux through the domain boundary (the inlet and outlet).

Materials: Although the geometries of the CFD simulation models were duplicated from the dynamic thermal simulation models [Figure 7], the entire building envelopes for the CFD models were defined as timber material properties and the ground surface to be of gravel-filled soil. The raised floor and air infiltration were not considered in the CFD simulations. The material properties used in the CFD simulations are shown in Table 6 (see Appendix).

Microclimate data: The simulation time and date were selected from the location of Myanmar – the longitude of 21.96°N , the latitude of 96.09°E and the UTC of $+ 6:30$. The intensity of the solar radiation, air velocity, air turbulent intensity, the ambient temperature and the ground roughness conditions were set based on available weather data. The boundary temperatures of the building fabric and the initial temperatures were assumed to be the same outdoor dry bulb temperature.

The typical weather file of Mandalay showed that 24.61% of a year fell between the temperature range of 30°C and 36°C , which can be considered a high-temperature range. For instance, the CIBSE Guide A (2015) [38] has recommended that the internal operative temperature should not exceed 30°C in a free-running building. In order to understand a high outdoor air temperature range effect on its related indoor air temperature and airflow, two temperature variables – 30°C and 36°C – were used in the CFD simulations.

The ASHRAE Standard 55 (2013) [39] has recommended that the acceptable operative temperature limit in occupant-controlled, naturally conditioned spaces can be increased up to 2.2°C at the average airspeed 1.2 m/s . The typical weather file of Mandalay showed that 26.79% of a year had wind speeds of between 0.15m/s and 1.2m/s , while 33.56% of a year had wind speeds of between 1.2m/s and 3m/s . Therefore, two variables of wind speeds (1.2m/s and 3m/s) were considered for use in the CFD simulations. Regarding the radiation models, two

sets of the macroclimate entities shown in Table 2 were considered, which referred to the typical weather year data of Mandalay. Therefore, the CFD simulation experiments were set to compare 32 isothermal scenarios – two roof typologies for two ventilation modes (with gable vents or without gable vents), two temperature variables (30°C and 36°C as initial temperatures), two wind speed variables (1.2m/s and 3m/s), and two radiation conditions.

Table 2. Macroclimate entities for the radiation model used in the CFD simulations, data from typical weather file of Mandalay

Microclimate parameters	High radiation condition	Low radiation condition
Direct Normal Radiation (Wh/m ²)*	892	475
Diffuse Radiation (Wh/m ²)*	604	461
Sky cover (%)	0	50
Temperature variables	30°C and 36°C for both high and low conditions	
Wind speed variables	1.2 m/s and 3 m/s for both high and low conditions	

* Irradiation, the sum of irradiance over a time period, is the amount of solar energy falling on a unit area over a stated time interval which is expressed in Wh/m².

4. Results of the simulation studies

The results of IESVE simulations were presented on an annual basis, illustrating the indoor air temperatures for the three building typologies. The results of the CFD simulations were illustrated as indoor air temperature and indoor airflow for the two building typologies.

4.1. Simulation results from IESVE

Annual air temperatures: Figure 9 presents the results of the 24 scenarios that were generated for the indoor air temperatures of the occupied zones on an annual basis, based on a typical weather year of Mandalay. For the buildings with the material set-1, small differences between the outdoor and indoor air temperatures revealed that the indoor thermal environment of the simulated building had a close relation to the weather outdoors. On the contrary, there were considerable differences between the outdoor and indoor air temperatures in the results of the buildings with the material set-2. Virtually identical results from the two material sets showed that the maximum air temperatures of all buildings were negligibly different but the minimum air temperatures of the buildings with material set-2 were higher than those with material set-1.

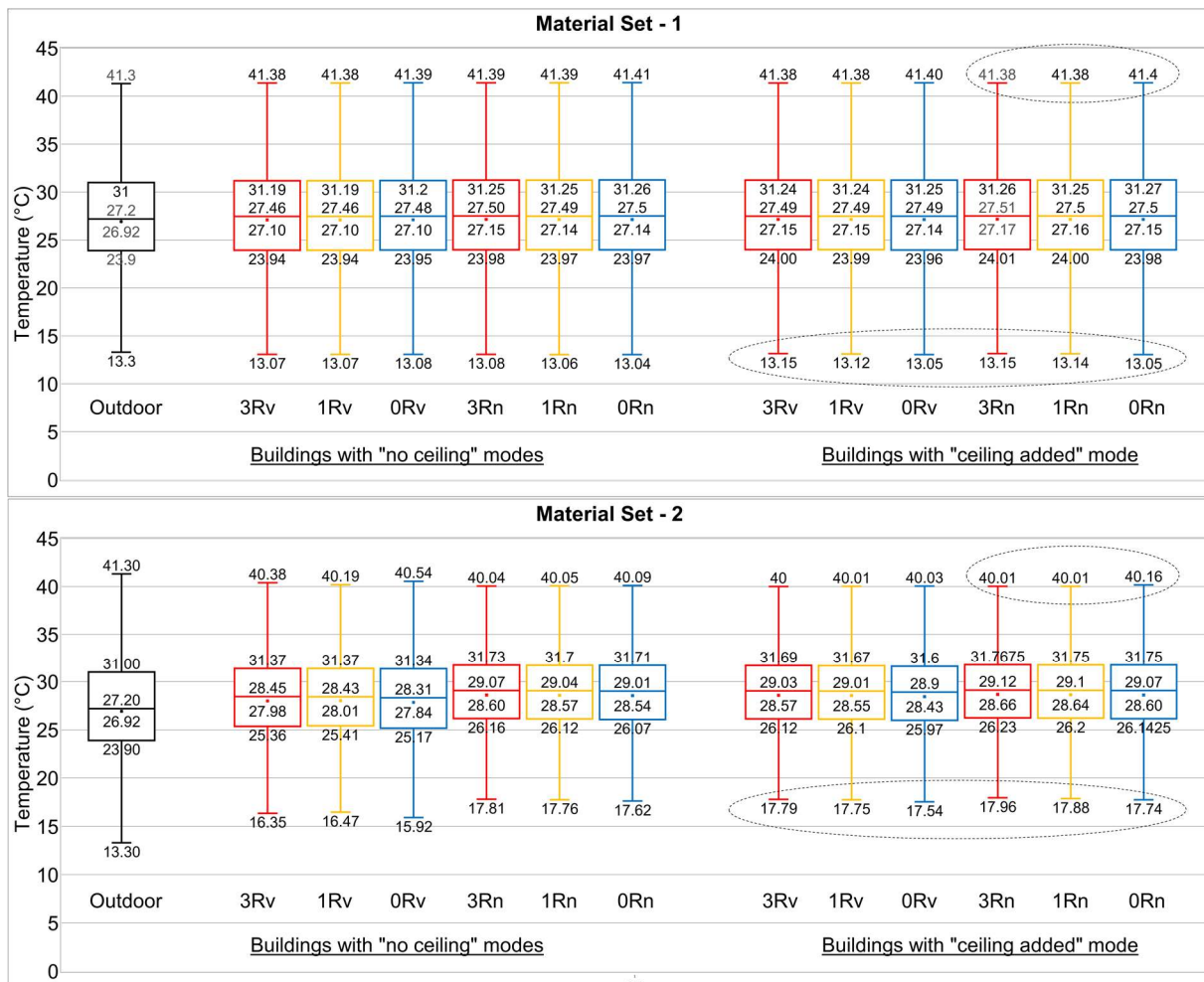


Figure 9. Air temperatures of the 24 scenarios simulated using a typical weather year for Mandalay

For instance, in Figure 9, the building 0Rn reached the maximum air temperature 41.4°C while the building 3Rn reached 41.38°C in the results of material set-1 (ceiling added mode). Similarly, the building 0Rn reached the maximum air temperature 40.16°C while the building 3Rn reached 40.01°C in the results of material set-2 (ceiling added mode). The material set-2 contained a cool roof effect from which the buildings could better offset the peak outdoor dry bulb temperature than the buildings with material set-1 were able to. Moreover, the buildings with material set-2 received shorter quartile lengths and higher median and mean values than the buildings with material set-1. It was also found that the values of the upper extremes for all scenarios were above 31°C. Therefore, the authors decided to check the percentage of a year above indoor air temperatures, with 31°C and 36°C as extreme cases.

Air temperatures above 31°C and 36°C: Figure 10 indicates that the buildings with material set-2 received a higher percentage of a year above indoor air temperature 31°C and maintained the lower percentage of a year above indoor air temperature 36°C. Conversely, the buildings with material set-1 received a lower percentage of a year above indoor air temperature 31°C and maintained a higher percentage of a year above indoor air temperature 36°C. The percentages of a year above 31°C and 36°C were increased in the buildings if there were no gable vents.

For instance, for the buildings with no ceiling in the material set-2, 31°C was found in the building 3Rv for 27.31% of a year above indoor air temperature, but this changed to 30.81% in the building 3Rn, as 3.5% difference. Moreover, the results of both material sets showed an increased percentage of air temperatures above 31°C and 36°C in all buildings when the ceilings were added but the gable vents were excluded. The results of Figure 9 and Figure 10 were generated for the occupied spaces, and the building geometries, internal gains and window opening times were fixed. Therefore, those different results of indoor air temperatures were due to the impacts of roof typologies, roof ventilation, ceiling modes, and building materials.

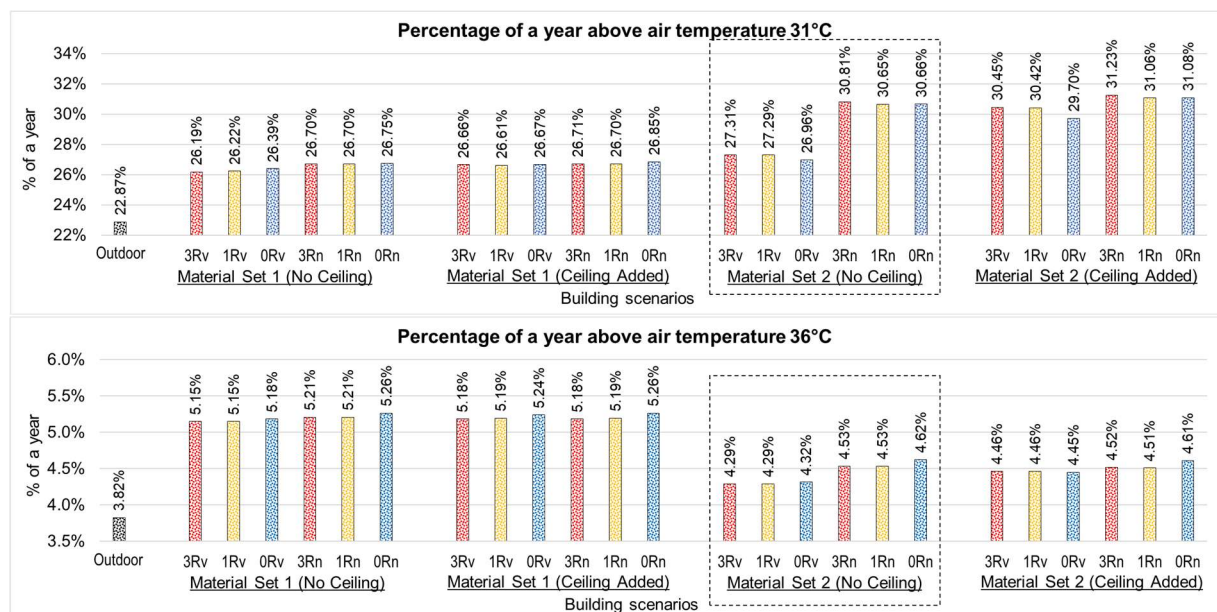


Figure 10. Air temperatures above 31°C and 36°C at the occupied spaces of each building, a typical weather year for Mandalay

Peak air temperatures: The results of Figure 11 were generated from the indoor air temperatures of all intermediate roof levels from the day when the air temperature reached the maximum value in a typical weather year. The results showed that the indoor air temperatures of the roof spaces were higher than the occupied space. As there were no internal gains in the occupied spaces of all buildings, a high indoor air temperature of roof spaces was due to its direct contact with the solar heat gain above the roof and the upward buoyant force of the hot air. Although the results of the buildings' indoor air temperatures of occupied space were unnoticeably different in all scenarios, their indoor air temperatures of roof spaces were significantly increased, but the increments were different due to ceiling mode, ventilation modes and building materials. In both material sets, the indoor air temperatures of roof spaces unnoticeably dropped when the ceilings were added but considerably increased when the gable vents were excluded. In both material sets, if the buildings had gable vents, the resultant indoor air temperature was lower in building 0Rv than in building 3Rv. On the contrary, in the material set-2, if the gable vents were excluded from the models, the building 0Rn resultant roof space's indoor air temperature was higher than in building 3Rn. For instance, as shown in Figure 11, in the material set-1 without ceiling mode, the roof space's indoor air temperatures of building 3Rv reached 41.89°C and of building 0Rv reached 41.64°C; building 3Rn reached 42.65°C while building 0Rn reached 42.44°C. In the material set-2 with the ceiling added mode, the roof space's indoor air temperatures of building 3Rv reached 42.18°C and building 0Rv reached 41.59°C; building 3Rn reached 42.02°C while building 0Rn reached 43.04°C.

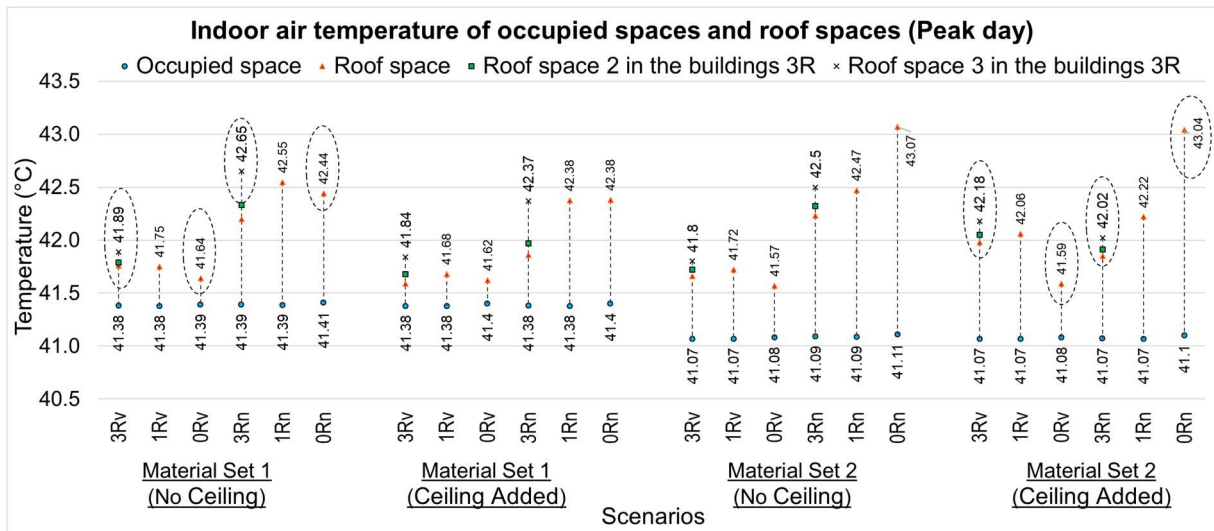


Figure 11. Indoor air temperatures of occupied space and roof spaces of each building – results for the day when the air temperature reached a maximum for a typical weather year

4.2. Simulation results from CFD

This section presents the results of the 32 isothermal scenarios that were investigated using CFD simulation; the results were generated from the vertical planes of each building with 1m interval that allowed us to compare the changes of indoor air temperatures and airflows along with the building height. The vertical planes of temperature profiles were generated using a normal angle at the inlet wind direction. The vertical planes of airflow profiles were generated from the plane which was parallel to the inlet wind direction.

Roof typologies: Figure 12 presents the indoor air temperatures' profiles and airflow profiles of two building typologies in which two ventilation modes were compared for the microclimate variables 36°C (temperature) and 3m/s (wind speed) from the vertical planes. Selecting samples for a high temperature (36°C) and wind speed (3m/s) for Figure 12 allowed us to compare a significant turbulence indoor airflow and temperature changes along the vertical planes. The results showed that the indoor air temperatures of the building 3Rn were lower than those of the building 0Rn up to 2.5m height. For instance, the indoor air temperatures were found at 2m height as 37°C in the building 3Rn and at 38°C in the building 0Rn. However, along the vertical planes, 2.5m onward, the building 3R maintained a higher indoor air temperature than the building 0R. On the contrary, the indoor air temperatures of the

building 3Rv was found to be 43.6°C at 13.5m height (near the roof) and the indoor air temperatures of the building 0Rv was found to be 38.4°C at 9m height (near the roof), from which the roof's space temperature difference was found to be 5.2°C. It was also clear that the lack of gable vents caused high indoor air temperatures. For instance, the indoor air temperatures of the building 3Rv were found to be 43.6°C at 13.5m height (near the roof); at that time the indoor air temperatures of the building 3Rn was found to be 50.7°C.

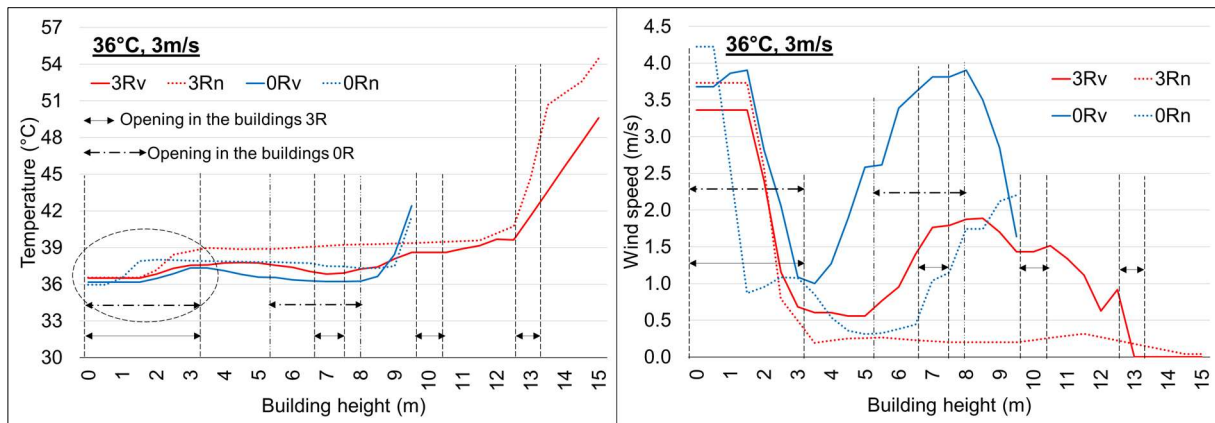


Figure 12. Indoor air temperatures profiles and airflow profile of two building typologies with two ventilation modes at high radiation conditions of the observed vertical planes

Unlike temperature profiles, significant differences between the buildings with gable vents and without gable vents were found in the wind speed profiles. The different profiles of buildings 3Rn and 0Rn revealed that the impacts of building height and roof typologies had greater impacts on the airflow profiles than on the temperature profiles. The upstream airflow of building 0Rv reached to about 8m in height, where there was a large area of gable vent; however, the airflow instantly dropped near the roof. On the contrary, the airflow in building 3Rv accelerated along with its location of gable vents, but created a lower airflow than building 0Rv attained, the lowest of which was near the roof.

Indoor air temperatures: The indoor air temperature profiles shown in Figure 13 were generated for a high radiation condition for two building typologies with two ventilation modes. In all buildings, the indoor air temperatures were significantly inclined from about 2.5m height onwards. The results revealed that there was temperature increment at the top of the roof

and boundary of the envelope, which was clearly indicated with green and light blue colours. The results showed that the indoor temperatures at the lower height of the building 3R were closely related to its initial temperatures and the outdoor microclimates than was the case with building 0R. For instance, at the outdoor microclimate scenario 30°C with 1.2m/s, the indoor temperatures of the building 0Rn and building 3Rn were 32.4°C and 31°C, respectively at 1m height. Among all results, the building 3Rn with a low airspeed for the outdoor microclimate showed the worst-case scenarios. For instance, the indoor air temperatures of the building 3Rn were found to be 56°C at 14m height (near the roof) for 36°C, 1.2m/s scenario.

Indoor airflow: Following the same approach presented for the indoor air temperature profiles, the indoor airflow profiles shown in Figure 14 were generated for a high radiation condition. The results revealed that there was scope for air turbulence in the buildings with gable vents. The results also showed that the speed of indoor airflow dropped beyond the opening height of building 3Rn that even caused very still air conditions near the top of the roof. Unlike building 3Rn, some turbulence was found at the top of building 0Rn. When there was wind flowing through the gable vents, turbulent conditions were found in both buildings 3Rv and 0Rv aligned with the height of the gable vents. For instance, in building 3Rv for the profile of 36°C with 3m/s, the speed of indoor airflow dropped to 0.6m/s at 4m height but increased to 1.9m/s at 8.5m height. Although both buildings 3Rv and 0Rv had the same indoor air volumes and gable vent areas, a greater airflow can be observed in the building 0Rv, which was caused by a single inlet of wind.

Radiation models: Figure 15 compares the results of two radiation conditions for the building 3Rn (solid lines for low radiation conditions and dash lines for high radiation conditions), where the intensity of radiation was differentiated by the values of sky cover, direct normal radiation and diffuse radiation, as shown in Table 2. In the same building, if the initial temperature, the outdoor dry bulb temperature and wind speed were fixed, the scenario with a

low radiation condition received a lower indoor temperature than the scenario with a high radiation condition. If the occupied spaces were considered for 2m height, for the profile of 30°C with 1.2m/s, the indoor air temperature was found to be 31.5°C in low radiation conditions, it changed to 32.2°C in the high radiation conditions that caused 0.7°C difference. The more the building height increased, the higher the temperature increment was found between two radiation conditions. For instance, for the profile of 30°C with 3m/s, the indoor air temperature of low radiation conditions was found to be 34.2°C at 12m height, but the indoor air temperature of high radiation conditions was found to be 32.6°C at 12m height, which caused a 1.6°C difference. For instance, for the profile of 36°C with 3m/s, the indoor air temperature of low radiation conditions was found to be 40.2°C at 12m height, but the indoor air temperature of high radiation conditions was found to be 38.6°C at 12m height, causing a 1.6°C difference. When the two radiation conditions were compared, a small temperature difference (0.7°C) was found when the outdoor microclimate entities were 30°C with 1.2m/s, but a large temperature difference (1.6°C) were found when the outdoor microclimate entities were at 30°C with 3m/s and 36°C with 3m/s. The results of the temperature differences between the two radiation conditions revealed that there was a considerable heat gain from the solar radiation in the studied climate.

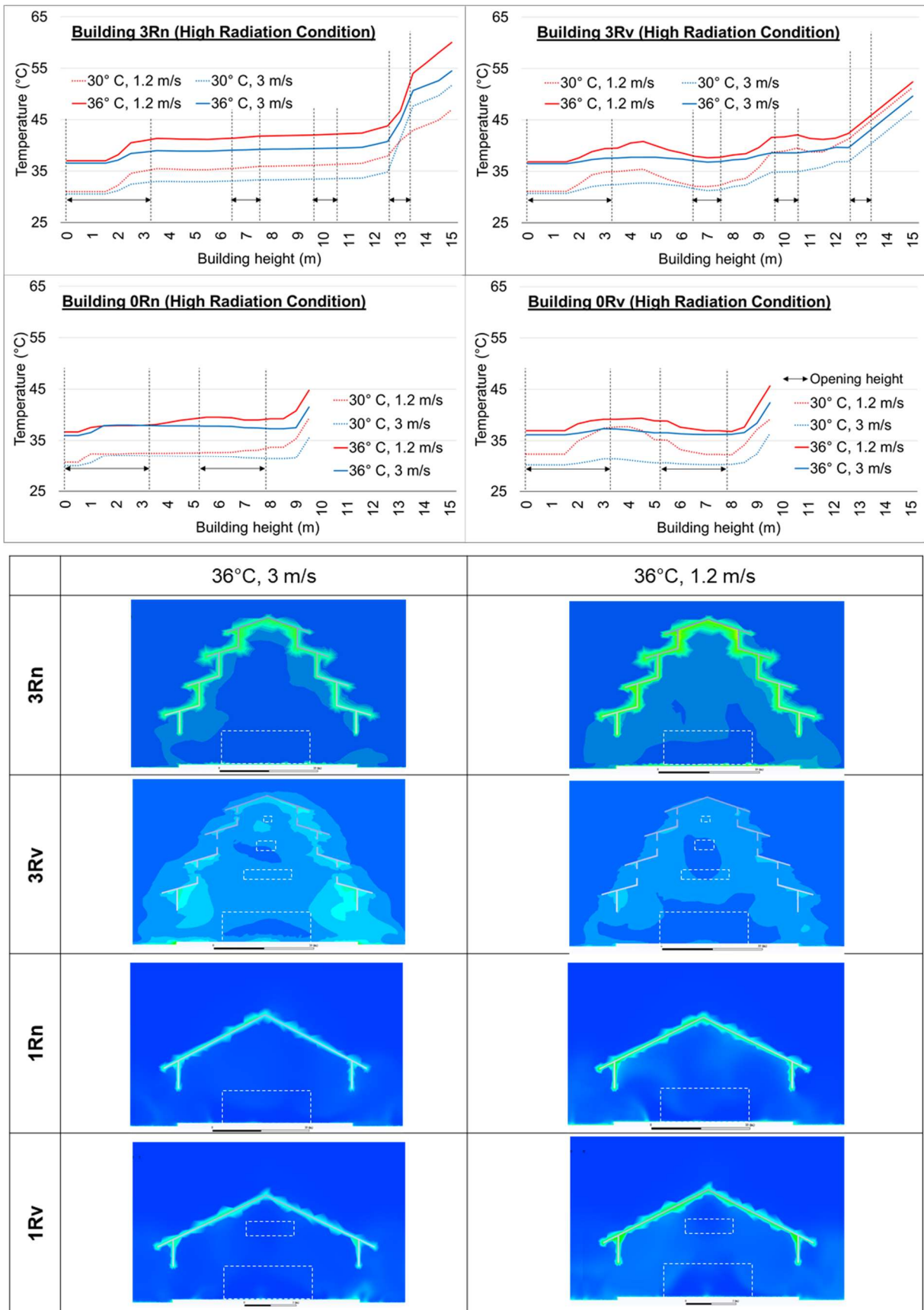


Figure 13. Indoor air temperature profiles of two building typologies with two ventilation modes considering high radiation conditions on the observed vertical planes

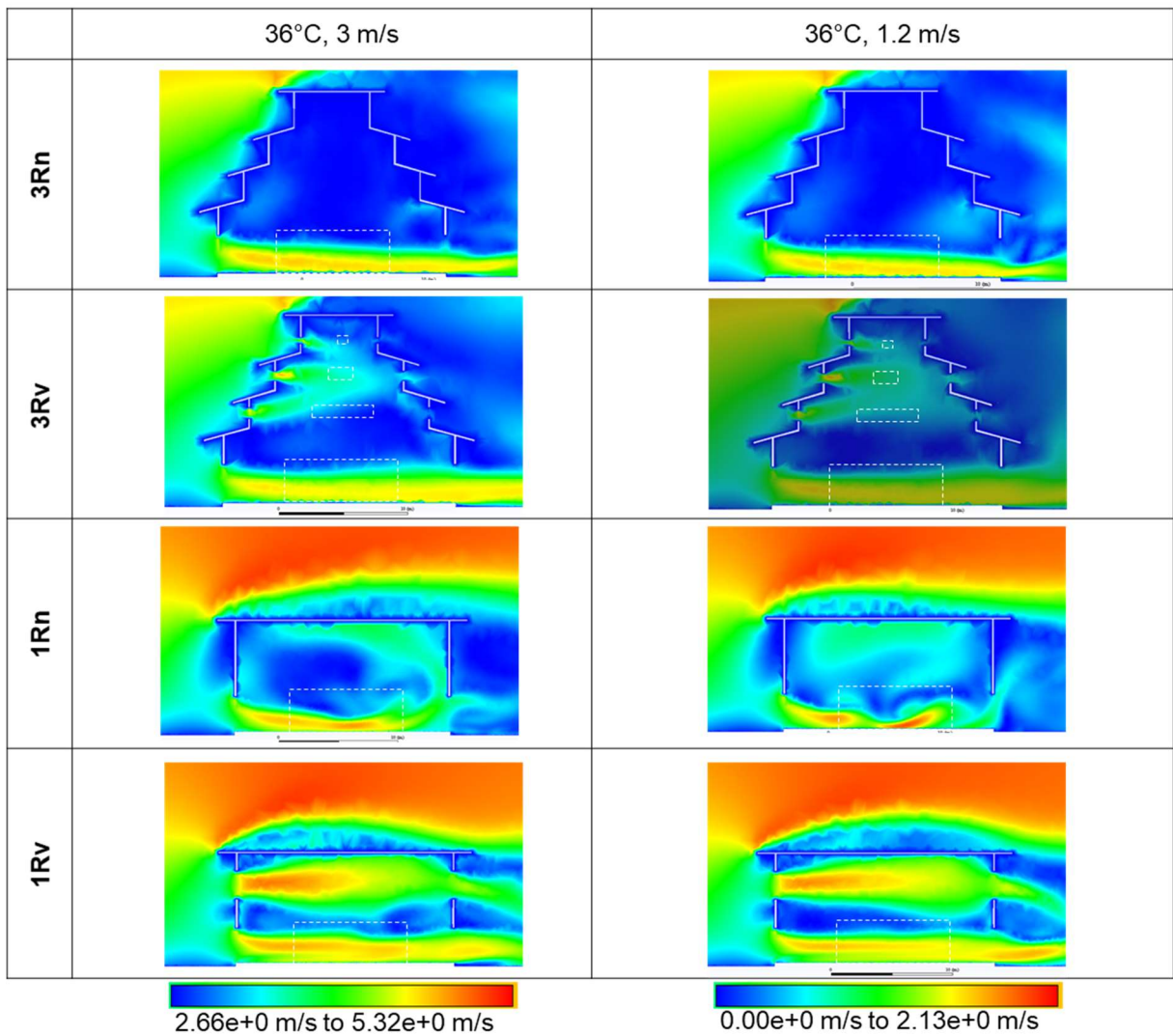
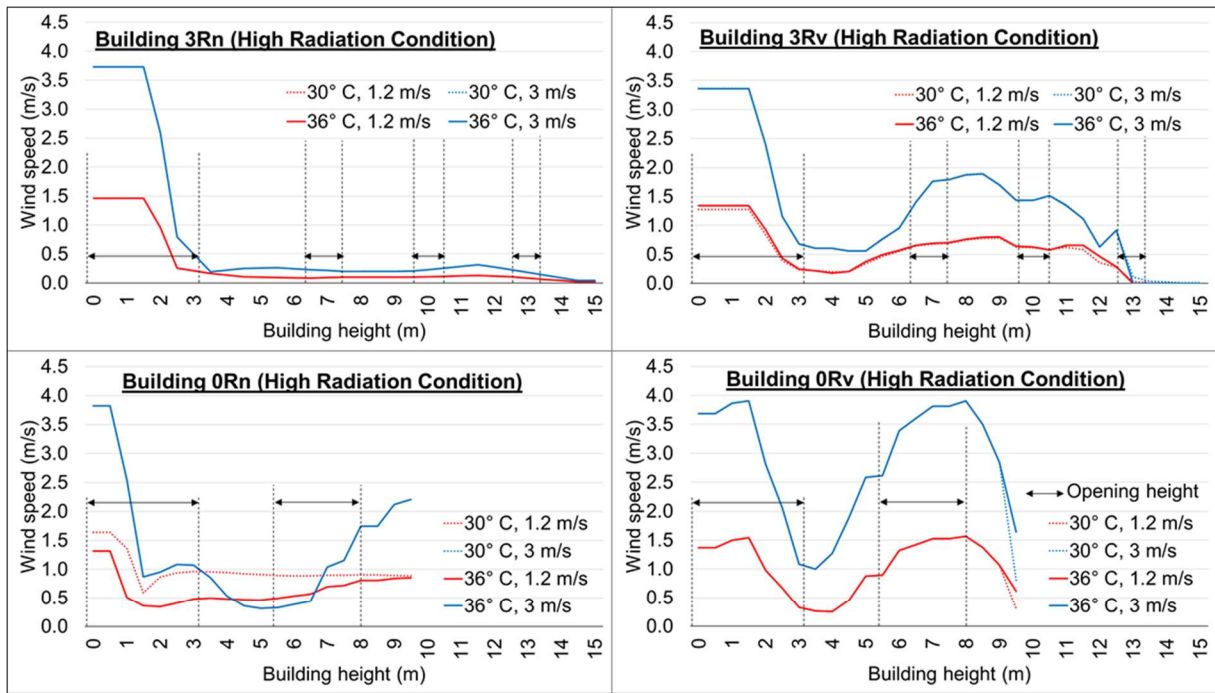


Figure 14. Indoor airflow profiles of two building typologies with two ventilation modes considering high radiation conditions on the observed vertical planes

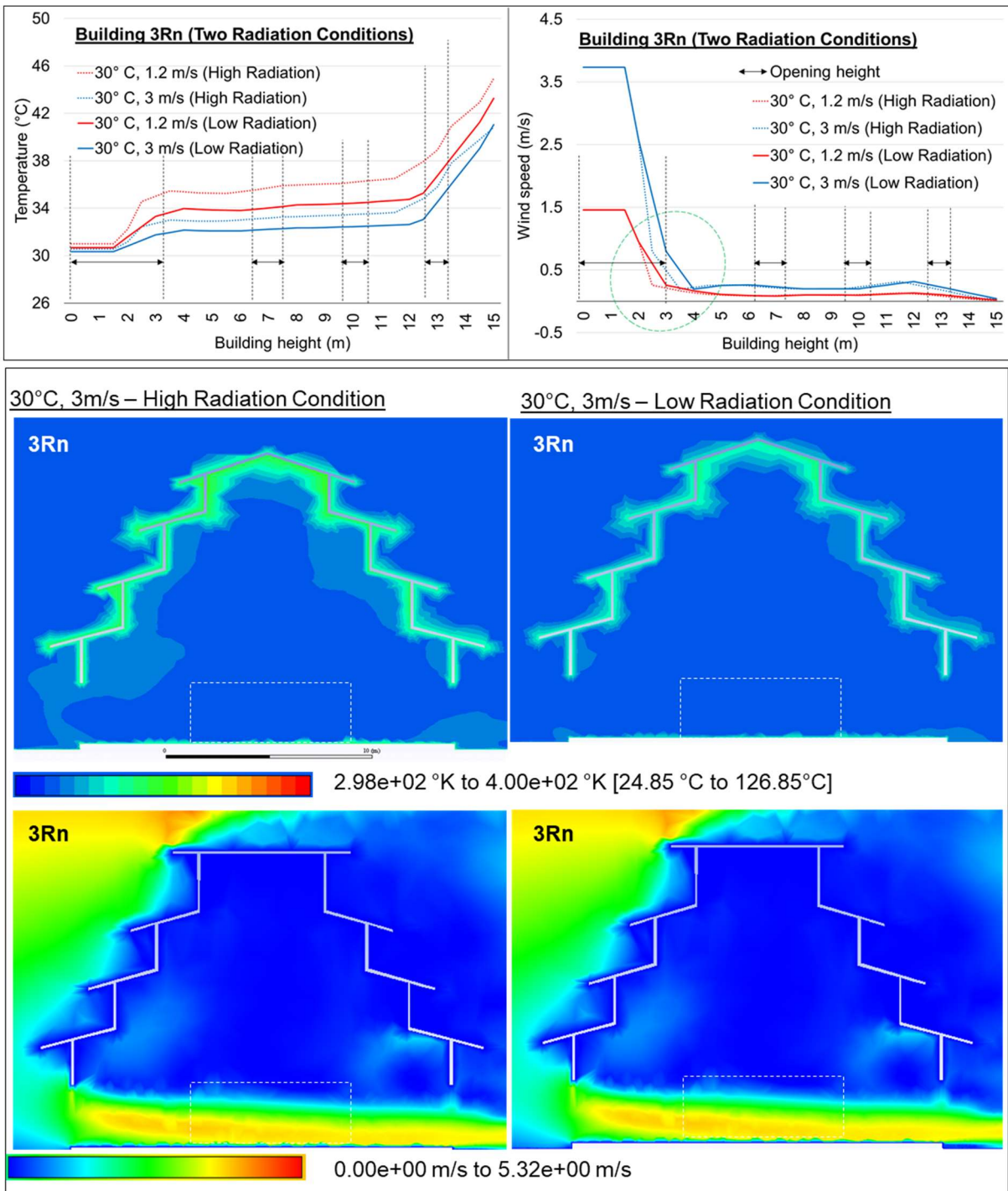


Figure 15. Comparison of high and low radiation conditions for the building 3Rn

5. Discussion

The factors that impact on the resultant building microclimates considering the prescribed scenarios and combinations of conditions are complex. Therefore, the findings for the key questions were grouped under headings, as follows.

5.1. Building materials

Distinct outcomes were observed between the material set-1 (thatch roof and timber walls) and material set-2 (metal roof and brick walls) considering annual air temperatures in the occupied spaces [Figure 9]. The material set-1 contained lightweight vernacular materials such as timber. The buildings with material set-1 presented a high percentage of a year above 36°C [Figure 10], which revealed that buildings with vernacular materials might be vulnerable to high and extreme temperature conditions. The results presented for the material set-1 are in agreement with the study by Nicol et al. [40]: if buildings have poor insulation characteristics or are lightweight, with low thermal capacity, they are likely to produce uncomfortable indoor temperatures during hot summers. The material set-2 contained a cool roof effect with less solar absorptance value (high reflectance) and high thermal capacity in the walls. Regardless of the differences in roof typologies, the use of material set-2 caused a higher annual mean temperature and a higher minimum air temperature in the occupied spaces [Figure 9]. Therefore, the buildings with material set-2 presented a higher percentage of a year above 31°C but a lower percentage of a year above 36°C than the material set-1 [Figure 10]. In agreement with this, two years of continuous monitoring work undertaken in Italy also revealed that the buildings with cool roof effect had better capability to offset a higher outdoor dry bulb temperature than a roof with high solar absorptance [41]. The highest indoor air temperature in the roof spaces of building 0Rn was observed in the results of material set-2; however, in both material sets, the highest indoor air temperature was observed in the roof spaces of the building 3Rv compared to the building 0Rv [Figure 11]. The simulation results from IESVE revealed that the thermal performances of the studied buildings were more altered by the building envelope materials and roof ventilation mode rather than by roof typologies.

5.2. Roof typologies and roof ventilation

In the IESVE simulations, building 3R presented a higher annual mean and median value but a lower maximum air temperature than building 0R [F9]. Moreover, the occupied space of the building 3R maintained a slightly lower percentage of a year above air temperature 31°C and 36°C than the buildings 1R and 0R when using the material set-1 [Figure 10]; however, differences in their results were negligible when roof typologies were considered. Regarding the roof space's air temperature, building 3R presented higher temperatures than building 0R regardless of gable vents modes in both material sets [Figure 11].

In the CFD simulations, the results showed that the indoor air temperatures of building 3Rn were lower than those of building 0Rn up to 2.5m height; however, along the vertical planes from 2.5m onward, building 3R maintained a higher indoor air temperature than the building 0R did [Figure 12]. The CFD results also showed that the building 3R maintained a higher indoor air temperature than the building 0R along the vertical planes of 2.5m onward.

Both IESVE and CFD simulations demonstrated good agreement, but findings conflicted for the building 3R, the traditional building with the multistage roof had lower air temperature up to 2.5m height but a higher roof space air temperature compared to the buildings with a single gable roof.

5.3. Response to tropical climates

Roof ventilation and roof typology play roles in removing hot air from a naturally ventilated building in the tropics. In this study, the CFD results suggested that building 3R could keep a lower air temperature up to 2.5m height. The results also demonstrated temperature differences between two radiation conditions, revealing considerable heat gain from the solar radiation in the studied climate [Figure 15]. This suggests that the buildings with multistage roofs have the benefit of being able to reduce the incidence of radiated heat gain. However, in order to avoid high air temperature in the roof space, gable vents should be used

to remove the hot air. Ameer et al.'s study [42] revealed that a narrowed roof in a building excels in providing a lower mean age of air and higher air change effectiveness and also creates a considerable roof height and less internal air volume. A similar concept was found in Myanmar's traditional buildings with a multistage roof that use an abstract roof curve to reduce the size of intermediate roof structures. Furthermore, one should not forget that the buildings with multistage roofs enable the relocation of the gable vent to the centre of the buildings, which allows for quicker removal of hot air quickly. In addition to the roof form, the simulation results revealed that the use of gable vents would be more effective in the buildings with multistage roofs if their building envelopes have material set-2.

The uncomfortably high air temperature in roof spaces revealed why the roof spaces of the ancient Myanmar buildings were unoccupied. Similar study done in the CFD simulations, which investigated the indoor air quality and thermal performance of a windcatcher building, showed a high air temperature near the top of the building [43].

Although the roof spaces of the buildings with multistage roofs were inherently vulnerable to overheating, the results of this study inform us that the indoor air temperatures of the occupied spaces for all simulated buildings closely responded to the outdoor air temperatures. Although the buildings with multistage roof has roof ventilation for passive cooling, the occupied spaces of the buildings with multistage roofs might be at risk of thermal discomfort because of both, extreme summer overheating and increased annual mean air temperature, due to the pervasive threat of the climate crisis. Similar results for Geodesic dome building in hot climates [44] also revealed that natural ventilation using roof vents cannot satisfy thermal requirements during hot summer periods and complementary cooling solutions should be considered.

5.4. Limitations

To date, very limited literature was found for the thermal performance design strategies used in Myanmar's vernacular architecture. Therefore, to the best of the authors' knowledge, this study might be one of the first to investigate the effects of the present climate conditions on the thermal performance of buildings with multistage roofs. It was impossible to capture the rich diversity of Myanmar cultures and customs as they developed through history within two simulation experiments presented in this paper; however, it was necessary to set the workable scope to investigate the difference between the buildings with a multistage roof and the buildings with a single gable roof in terms of their thermal performance. With this pressure in mind, the results of both simulations were generated as a single zone for the entire building with various prescribed, fixed assumptions. It is necessary to note acknowledge other limitations of this study as follows.

In both simulation studies, the size and shape of the buildings were treated as equal length and width, and 1.5m eave for roof shading. It is also important to note that the aim of using the sample size of buildings in this paper was to compare differences between three-stage multi-tier roofs and a single gable roof; therefore, a more realistic roof size for Myanmar's traditional building might be considered for application, as shown in Figure 4 and Figure 5. The weather file used in the IESVE simulations was unable to generalise to the whole country as Myanmar extends through 18 degrees of latitude that results in different climate zones. The CFD simulations were generated by using an isothermal situation; therefore, the exterior air temperature fluctuation, natural wind direction and wind speed changes over time were out of the scope of work for the CFD simulations. All these factors are difficult to put together in one study, yet nevertheless are important considerations for the building microclimate. Although the simulation theories used in this study were well-established [28, 30, 34-37], ideally input data and results should be validated with real-world data, for which further studies are

necessary. Nevertheless, the simulation studies presented in this paper can be a platform for further Myanmar vernacular architecture research, both for the art and history and for the building thermal performance design and building microclimates for the present climates.

6. Conclusion

When investigating the thermal performance of buildings with multistage roofs, several building parameters and microclimate conditions should be considered, as well as their impacts on indoor air temperatures and airflow. In the present study, the author used three buildings typologies with two ventilation modes to compare the impacts of building materials and different microclimate variables on the indoor thermal performance. When evaluating the thermal performance of the selected roof typologies, distinct results were observed when two different material sets were used; however, the thermal performances of the building with multistage roofs and the building with a single gable roof were more impacted by the use of different ventilation modes.

As [Oliver \(1986\)](#) asserted, the technological merits of vernacular traditions do need to be studied and understood, and the extent of vernacular knowhow does demand to be examined and recognised. The findings showed that Myanmar's vernacular buildings with multistage roofs offer an opportunity to improve indoor comfort in tropical weather because of their adaptability for roof ventilation through gable vents, and the use of an abstract roof curve to divide the number of tiers and to reduce roof internal air volume. If the grandness of the ancient Myanmar multistage roof is to be appreciated, it is not only because of its fine art and semiotic values; what should also be honoured is its capability to manage the hot, stale air in the roof structure from the use of simple building physics and geometry.

Appendix

Table 3. Material properties used in the IESVE simulations [28, 38]

	T	λ	D	Cp	U	Cm	SA
Material Set 1							
Thatch roof	300	0.07	240	180	0.2170	7.66	0.70
Timber floor	25	0.13	900	2000	2.9240	22.50	-
Timber wall	25	0.13	900	2000	2.9240	22.50	0.55
Timber ceiling	25	0.165	650	1600	2.7295	13.00	-
Timber window	40	0.130	900	2000	2.1863	36	-
Material Set 2							
Metal roof	15	0.19	960	837	2.3735	27.50	0.30
Concrete floor	500	-	-	-	0.7957	174.72	-
		Screed	0.41	1200	840		
		Sand	0.35	2080	840		
Brick wall	250	-	-	-	1.6692	124.60	0.55
		Plaster	-	600	1000		
		Brick	-	1700	800		
Timber ceiling	25	0.165	650	1600	2.7295	13.00	-
Glazed window	12	-	-	-	5.75	-	-
T = Total thickness [mm]; λ = Conductivity [W/(mK)]; D = Density [kg/m ³] Cp = Specific heat capacity [J/(kg.K)]; U = Thermal transmittance [W/m ² K] Cm = Thermal mass [kJ/(m ² K)]; SA = Outside surface Solar absorptance							

Table 4. Summary of the CFD model boundary conditions

Boundary condition	Set value
Algorithm	Simple
Time	Steady-state
Solver type	Pressure based
Discretisation Scheme	Second-order upwind
Turbulence model	Standard k-epsilon
Near wall	Standard wall functions
Velocity inlet	ABL profile (see Figure 16)
Pressure outlet	0 Pa

Table 5. Mesh characteristics of the buildings for CFD simulations

Buildings	Gable Vents contained	Elements	Nodes	Average skewness	Average orthogonal quality
3Rv	Yes	1015111	1408084	0.25148	0.74723
3Rn	No	1463635	2032705	0.24186	0.75686
0Rv	Yes	1599544	2226556	0.22755	0.77114
0Rn	No	1556506	2168641	0.22680	0.77188

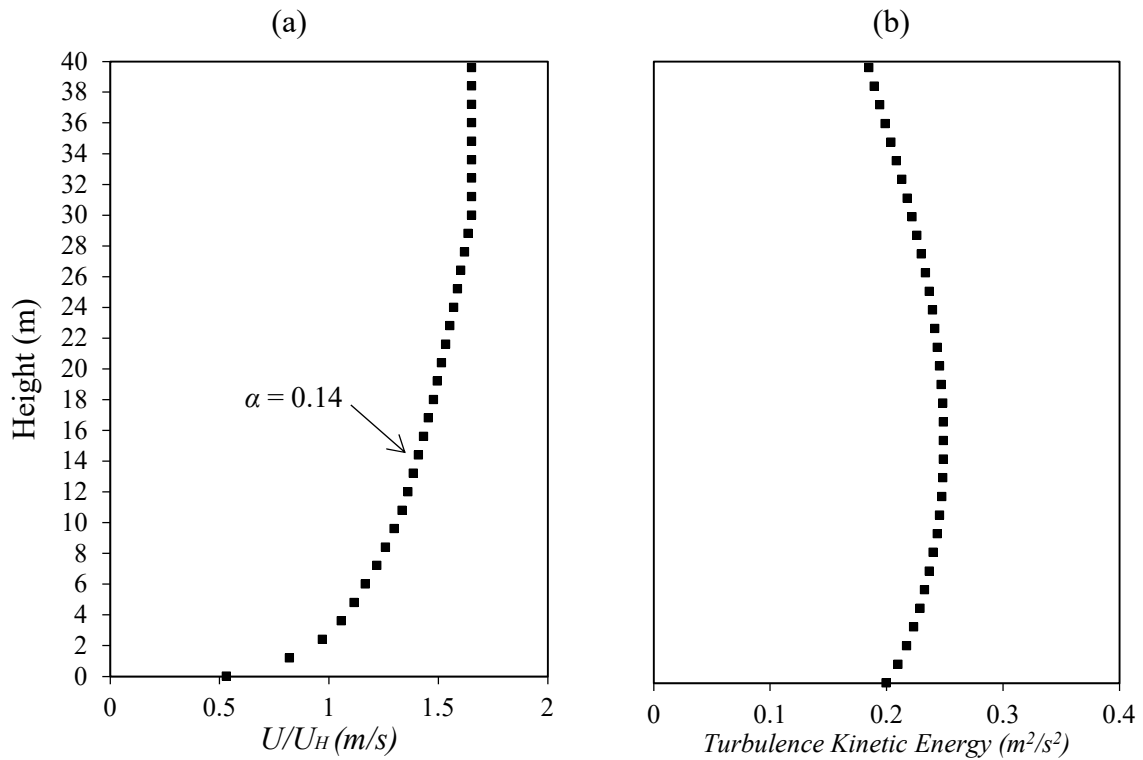


Figure 16. (a) Velocity profile; (b) Turbulent kinetic energy profile of approach wind flow [46]

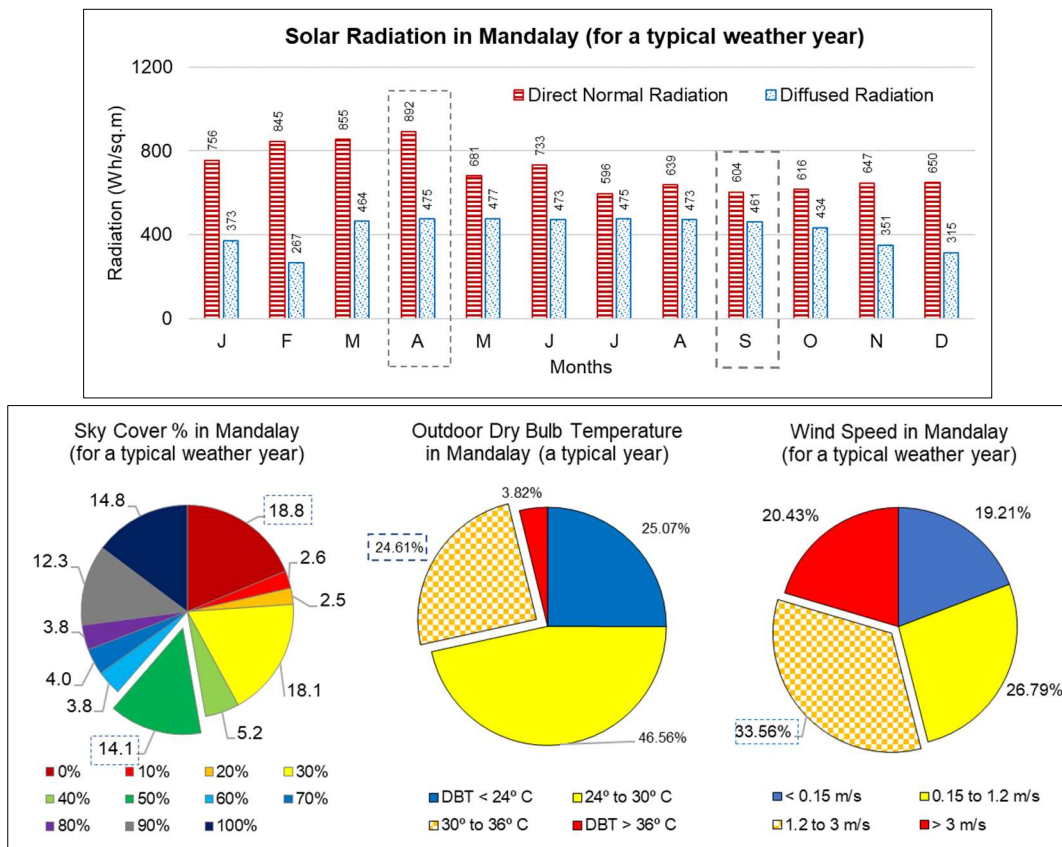


Figure 17. Microclimate entities of Mandalay in a typical weather year [30]

Table 6. Material properties of air and building materials used in CFD simulations

Material properties	Air	Timber (Building)
Density (kg/m ³)	1.225	900
Cp (Specific heat) (j/K-.kg)	1006.43	2000
Thermal conductivity (w/m-k)	0.0242	0.13

Reference

- [1] Harvey, G. E. (1925) *History of Burma: From the Earliest Times to 10 March 1824, the Beginning of the English Conquest*. London: Longmans, Green and Co.
- [2] Myint, Tin Win (1990) *Investigation of Pyatthat*. in Burmese language. Yangon: unknown.
- [3] Falconer, John, et al. (2000) *Burmese Design & Architecture (Photography by Luca Invernizzi Tettoni)*. Singapore: Petiplud Editions (HK).
- [4] Harmeling, Sven; Witting, Maximilian; Bals, Christoph, and Kreft, Sonke (2011) *Global Climate Risk Index 2011. Who Suffers Most From Extreme Weather Events? Weather-related Loss Events in 2009 and 1990 to 2009*. www.germanwatch.org/cri: Germanwatch e.V.
- [5] Eckstein, David; Kunzel, Vera; Schafer, Laura, and Wings, Maik (2019) *Global Climate Risk Index 2020. Who Suffers Most From Extreme Weather Events? Weather-related Loss Events in 2018 and 1999 to 2018*. Bonn, Germany: Germanwatch e.V.
- [6] Zune, May; Rodrigues, Lucelia Taranto and Gillott, Mark (2020) *Vernacular Passive Design in Myanmar Housing for Thermal Comfort*. Sustainable Cities and Society, 54 (DOI: <https://doi.org/10.1016/j.scs.2019.101992>), pp.-.
- [7] Zune, May; Rodrigues, Lucelia Taranto and Gillott, Mark (2018) The Resilience of Natural Ventilation Techniques in Myanmar's Vernacular Housing, In: Ng, Edward, Fong, Square, and Ren, Chao (ed.) *Passive and Low Energy Architecture Conference: Smart and Healthy within the 2-degree Limit*, 10-12 December, Hong Kong. pp.513-518.
- [8] Allen, Edward (1969) *Stone Shelters*. Cambridge, MA: The MIT Press.
- [9] Ozdeniz, M. B., et al. (1998) *Vernacular Domed Houses of Harran, Turkey*. Habitat International, 22 (4), pp.477-485.
- [10] Baran, Mine and Yilmaz, Aysel (2018) *A Study of Local Environment of Harran Historical Domed Houses in terms of Environmental Sustainability*. Journal of Asian Scientific Research, 8 (6), pp.211-220.
- [11] Nelson, Steven (2007) *From Cameroon to Paris: Mousgoum Architecture In and Out of Africa* Chicago and London: University of Chicago Press.
- [12] Hurstwic (1999-2019) *Turf Houses in the Viking Age*. Available from: http://www.hurstwic.org/history/articles/daily_living/text/Turf_Houses.htm [Assessed 1 May 2019].
- [13] Domenig, Gaudenz (2008) Variation in Karo Architecture, from *Indonesian House*, In. Schefold, R. and Nas, Peter J.M. (ed.), The Netherlands: KITLV Press, pp.49-99.
- [14] Bakken, Kristin (2016) *Preserving the Stave Churches Craftsmanship and Research*. Estonia: Pax Forlag.
- [15] Ministry of Construction (1993) *Kanbawzathadi Palace Reconstruction*.
- [16] Sein, Myo Myint, et al. (1970) *Monastery from Late Konebaung Dynasty*. University Pyin-Nyar-Pa-Day-Thar Paper, 5 (3), in the Burmese language. pp.269-292.
- [17] Zune, May (2019) *Vernacular houses in Asia, Africa and Europe* Photography courtesy of Berthold Werner (Trulli house), Sarah_c_murray (Beehive Houses), Chris Park

- (Chibotte), J. and M.F. Ostorero (Mugsum Mud Huts), Treeaid (Cliff of Bandiagara), Thomas Ormston (Viking Longhouse Stöng), TeeJe (Batak house), Lucie Debelkova (Mongolia's Yurts), Zereschk (Ab-anbar), Daisy Hook (Ma'dan Reed Houses), Nina Sabnani (Gujarat house).
- [18] Timeanddate (1995) *World Temperatures - Weather Around The World*. Available from: <https://www.timeanddate.com/weather/> [Assessed 8 October 2019].
- [19] EnergyPlus (NREL), National Renewable Energy Laboratory (1996). *Weather Data for More Than 2100 Locations*.
- [20] Rubel, Franz and Kotteck, Markus (2010) *Observed and Projected Climate Shifts 1901-2100 Depicted by World Maps of the Köppen-Geiger Climate Classification*. *Meteorologische Zeitschrift*, 19 (2), pp.135-141.
- [21] Fraser-Lu, Sylvia (1994) *Burmese Crafts: Past and Present*. USA: Oxford University Press.
- [22] Myint-U, Thant (2008) *The River of Lost Footsteps: A Personal History of Burma*. New York: Faber & Faber.
- [23] Bansal, Ben; Fox, Elliott and Oka, Manuel (2015) *Architectural Guide Yangon*. Berlin: DOM Publishers.
- [24] Hluttaw Brochure Working Group (2017) *Hluttaw Brochure*, Nay Pyi Taw: The Republic of the Union of Myanmar Hluttaw.
- [25] Lim, J.Y (1987) *The Traditional Malay House: Indigenous and traditional knowledge and practices*.
- [26] Soflaei, Farzaneh; Shokouhianb, Mehdi and Shemiranic, Seyed Majid Mofidi (2016) *Traditional Iranian Courtyards as Microclimate Modifiers by Considering Orientation, Dimensions, and Proportions*. *Frontiers of Architectural Research*, 5 (2016), pp.225-238.
- [27] Du, Xiaoyu; Bokel, Regina and Dobbelsteen, Andy van den (2014) *Building Microclimate and Summer Thermal Comfort in Free-running Buildings with Diverse Spaces: A Chinese Vernacular House Case*. *Building and Environment*, 82 (2014), pp.215-227.
- [28] IESVE Environment, IES Virtual (2015). *ApacheSim Calculation Methods*.
- [29] Jones, P J; Alexander, D K and Rahman, A M (1993) Evaluation of the Thermal Performance of Low-Cost Tropical Housing, In: (ed.) *International Building Performance Simulation Association*, Adelaide, Australia. pp.137-144.
- [30] Huang, J.Y; Su, F.X.; Seo, D.H., and Krarti, M. (2014) *Development of 3,012 IWEC2 Weather Files for International Locations (RP-1477)*. *ASHRAE Transactions*, 120 (1), pp.340-355.
- [31] Calautit, John Kaiser and Hughes, Ben Richard (2016) *A passive cooling wind catcher with heat pipe technology: CFD, windtunnel and field-test analysis*. *Applied Energy*, 162 (2016), pp.460-471.
- [32] Calautit, John Kaiser; Hughes, Ben Richard and Shahzad, Sally Salome (2015) *CFD and wind tunnel study of the performance of a uni-directionalwind catcher with heat transfer devices*. *Renewable Energy*, 83 (2015), pp.85-99.
- [33] Cebeci, Tuncer and Bradshaw, Peter (1977) *Momentum transfer in boundary layers*. New York: McGraw-Hill.
- [34] Franke, J., et al. (2004) Recommendations on the Use of CFD in Wind Engineering, In: *Proceedings of the International Conference on Urban Wind Engineering and Building Aerodynamics* (ed.) *COST Action C14, Impact of Wind and Storm on City Life and Built Environment*, May 5-7, 2004, Rhode-Saint-Genèse, Belgium. pp.C.1.1-C1.11.

- [35] Blocken, Bert; Stathopoulos, Ted and Carmeliet, Jan (2007) *CFD Simulation of the Atmospheric Boundary Layer: Wall Function Problem*. *Atmospheric Environment*, 41 pp.238-252.
- [36] Bottillo, S.; Vollaro, A. De Lieto; Galli, G., and Vallati, A. (2014) *Fluid Dynamic and Heat Transfer Parameters in an Urban Canyon*. *Solar Energy*, 99 (2014), pp.1-10.
- [37] Mavriplis, Dimitri J. (1999) *Large-scale Parallel Viscous Flow Computations Using an Unstructured Multigrid Algorithm*. Institute for Computer Applications in Science and Engineering (ICASE).
- [38] GVA/15 CIBSE Guide A (2015) *Environmental Design 2015*. Lavenham, Suffolk, UK: Chartered Institution of Building Services Engineers.
- [39] ANSI ASHRAE Standard 55 (2013) *Thermal Environmental Conditions for Human Occupancy*. USA: ASHRAE Standards Committee, the ASHRAE Board of Directors, and the American National Standards Institute.
- [40] Nicol, Fergus; Rudge, Janet and Kovats, Sari (2005) Safe and warm; effect of climate change on thermal comfort and health, from *Adapting Buildings and Cities for Climate Change: A 21st Century Survival Guide*, In. Roaf, Sue, Crichton, David, and Nicol, Fergus (ed.), An imprint of Elsevier: Architectural Press,
- [41] Pisello, Anna Laura and Cotana, Franco (2014) *The thermal effect of an innovative cool roof on residential buildings in Italy: Results from two years of continuous monitoring*. *Energy and Buildings*, 69 (2014), pp.154–164.
- [42] Ameer, Shazia Ahmed; Chaudhry, Hassam Nasarullah and Agha, Arouge (2016) *Influence of Roof Typology on the Air Distribution and Ventilation Effectiveness of Wind Tower*. *Energy and Buildings*, 130 (2016), pp.713-746.
- [43] Calautit, John Kaiser; Tien, Paige Wenbin; Wei, Shuangyu, and Calautit, Katrina (2020) *Numerical and experimental investigation of the indoor air quality and thermal comfort performance of a low energy cooling windcatcher with heat pipes and extended surfaces*. *Renewable Energy*, 145 (2020), pp.744-756.
- [44] Soleimani, Zohreh; Calautit, John Kaiser and Hughes, Ben Richard (2016) *Computational Analysis of Natural Ventilation Flows in Geodesic Dome Building in Hot Climates*. *Computation (MDPI)*, 4 (3), pp.31.
- [45] Oliver, Paul (1986) *Vernacular know-how*. *Material Culture*, 18 (3), pp.113-126.
- [46] Blocken, Bert (2015) *Computational Fluid Dynamics for urban physics: Importance, scales, possibilities, limitations and ten tips and tricks towards accurate and reliable simulations*. *Building and Environment*, 91 (2015), pp.219-245.

Endnote

¹ The immensely thick stone walls and dome of the Trulli houses create a pleasantly cool environment in the summer; however, the excess moisture in the air condenses while cooking; therefore, the inhabitants need to leave the doors and small windows open during the day to keep the interior dry and to remove the humid air inside the building.

² In a Beehive-shaped house, the hole at the sides of each conical dome serves as a chimney and a ventilation hole to remove the smoke and hot air that allows occupants to avoid the indoor moisture from the sun-

dried or burned clay brick envelope. Therefore, the inhabitants usually close the openings to prevent the extreme differences in the climate during the summer and the winter to maintain a comfortable indoor environment.

³ The stone and earth architecture of Dogon Country is set against the steep cliffs of Mali's Bandiagara escarpment.

⁴ Cameroon huts in Musgum are made of sun-dried mud.

⁵ The Viking longhouse begins with the construction of stone footings. Besides forming a firm base on which the house rests, they also keep the wooden structural elements of the house away from the soil, protecting them from rot.

⁶ The boat-shaped Batak longhouse has carved gables and large steeply pitched saddle back roof, and the main house is built on piles.

⁷ Stave churches are elaborately carved wooden houses of worship once common in north-western Europe. Stave building is a frame construction consisting of horizontal and vertical elements resting on the stone foundation on the ground. Stave churches with elevated naves have a number of staves, or nave posts, which stand separately in the interior and support the upper part of the construction. Heddal stave church is the largest surviving stave church with elevated naves in Notodden, Norway, which was probably built in the 1200s. Most stave churches were made of Scots pine and oak, which have an extreme density and are hard to find in present-day Norwegian forests; therefore, the excellent quality timber might be one of the reasons for those wooden buildings surviving in the Nordic climate for so many centuries.

⁸ Pyatthat in the Pali-Myanmar dictionary means 'a building with a series of roof tiers'. The word originated from the Sanskrit word 'Pa-Thar-Da', which means 'a building with pleasant sight.' Each tier is called "boun", and the numbers are always uneven to keep three or five or seven tiers, up to eleven. An intermediate box-like roof structure inserted between each tier is called "Le-baw".

⁹ Four types of multistage roofs can be categorised by historical dynasties: Pagan dynasty, first-Ava dynasty, Hanthawaddy dynasty, and Konbaung dynasty. The use of intermediate roof structures is more dominant in the Pagan and first-Ava dynasties. The use of a series of roofs is more powerful in the Hanthawaddy dynasty, which was developed for Kho-Nan-Cho design, which means there are the same length and width at every corner. The empire of King Bayinnaung extended to the Ayutthaya of Thailand in the Hanthawaddy Dynasty. Therefore, the use of a series of roofs has been developed in both countries.